Aerosp. Sci. Technol. 142 (2023) 108653

Contents lists available at ScienceDirect

Aerospace Science and Technology

journal homepage: www.elsevier.com/locate/aescte

Dynamic event-triggered attitude synchronization of multi-spacecraft formation via a learning neural network control approach

Qingxian Jia [a,*], Junnan Gao [a], Chengxi Zhang [b,c], Choon Ki Ahn [d,*], Dan Yu [a]

[a] College of Astronautics, Nanjing University of Aeronautics and Astronautics, 210016 Nanjing, China
[b] School of Internet of Things Engineering, Jiangnan University, Wuxi 214122, China
[c] Key Laboratory of Advanced Control for Light Industry Processes, Ministry of Education, Jiangnan University, Wuxi 214122, China
[d] School of Electrical Engineering, Korea University, Seoul 136-701, South Korea

ARTICLE INFO

Communicated by Chaoyong Li

Keywords:
Spacecraft formation
Attitude synchronization
Dynamic event-triggered
Learning neural-network control
Iterative learning algorithm

ABSTRACT

This paper addresses the robust attitude synchronization issue in a multi-spacecraft formation system subjected to limited communication, space disturbances, modeling uncertainties, and actuator faults. To accommodate limited inter-spacecraft communication, a dynamic event-triggered mechanism is designed to reduce the communication trigger frequency by dynamically adjusting the trigger threshold. Moreover, an event-based distributed self-learning neural-network control (SLN^{2}C) law is developed to guarantee robust attitude synchronization during multi-spacecraft formation. In the SLN^{2}C scheme, a learning radial basis function neural network (RBFNN) model is proposed to online approximate and compensate for lumped disturbances, in which an iterative learning algorithm with a variable learning intensity is adopted to update the weight matrix of the RBFNN model. Compared with the traditional fixed learning intensity, a variable one can reduce initial oscillation and weaken the saturation response. Numerical simulations and comparisons are performed to illustrate the effectiveness and superiority of the proposed event-based spacecraft attitude synchronization control method.

1. Introduction

Over the past two decades, spacecraft formation flying (SFF) has garnered significant attention due to its widespread aerospace engineering applications, that is, interferometric synthetic aperture radar (InSAR)-based Earth observation, distributed SAR-based reconnaissance, and deep space exploration [1,2]. Unlike large and complex spacecraft, the SFF system comprising multiple spacecraft has substantial advantages, such as high reliability, high robustness, and extensive function expansion capacity in space missions. Various spacecraft formations have been launched into orbit, such as the TanDEM/TerraSAR-X satellite project (Germany, 2008), the PRISMA satellite project (Sweden, 2010) and the Hongtu-1 satellite project (China, 2023). Attitude synchronization, like the essential attitude manipulation of a single spacecraft, is essential in spacecraft formation missions, such as beam pointing synchronization for InSAR satellites and beam ground splicing for distributed SAR reconnaissance [3,4]. During a formation mission, the relative attitudes of spacecraft must typically be maintained with high accuracy. Therefore, attitude synchronization control for SFF systems has become an increasingly attractive research topic [5–7].

For the on-orbit SFF system, space communication channels and bandwidth between spacecraft in formation are usually limited due to spacecraft costs, launch expenses, and wireless transmission capability. Moreover, with the rapid development of small spacecraft technology, low-cost small spacecraft formation has become an emerging trend during the past decade, also resulting in limited communication resources. Event-triggered sampling has emerged as a promising technique for reducing data transmission in multi-agent systems [8,9]. This technique triggers communication sampling only when prescribed events occur rather than at fixed sampling intervals, thereby reducing the communication interaction between agents. Accordingly, event-triggered control (ETC) mechanisms, characterized by aperiodic asynchronous communication and computation, have been widely studied for distributed SFF systems, with excellent progress being made [10–14].

For the multi-spacecraft formation system with indirect information flow, a state-irrelevant event-based attitude synchronization control method was studied in [10]. In [11], a distributed event-based attitude synchronization control approach was proposed for the SFF system with unknown disturbances and modeling uncertainties. An event-triggered

* Corresponding author.
E-mail addresses: jqxnuaa@nuaa.edu.cn (Q. Jia), gao_junnan@126.com (J. Gao), dongfangxy@163.com (C. Zhang), hironaka@korea.ac.kr (C.K. Ahn), yudan@nuaa.edu.cn (D. Yu).

https://doi.org/10.1016/j.ast.2023.108653
Received 15 July 2023; Received in revised form 29 August 2023; Accepted 27 September 2023
Available online 2 October 2023
1270-9638/© 2023 Elsevier Masson SAS. All rights reserved.

mechanism and sliding mode-based robust attitude coordinated control method were proposed in [12], where the non-existent solution on the event-triggered mechanism due to the discrete sliding mode surface was considered. Event-triggered mechanism-based attitude synchronization control of a multiple uncertain rigid SFF system over jointly connected networks was investigated in [13], where an adaptive observer-based ETC law was designed to achieve robust attitude synchronization. The periodic event-triggered mechanism-based coordinated control for Euler-Lagrange systems with modeling uncertainties and external disturbances was investigated and applied to attitude synchronization for multiple satellites in [14], where an adaptive neural network model was incorporated to update and compensate for modeling uncertainties. In the above-mentioned work, static event-triggered (SET) mechanisms that possess a fixed trigger condition with constant thresholds were adopted. This mechanism can initially alleviate the communication burden, but it results in unnecessary communication triggers and may lose packets containing essential information [15].

To address the drawbacks caused by SET mechanisms, dynamic event-triggered (DET) control strategies have been recently developed. The DET mechanisms adopt a dynamic trigger condition with a time-varying threshold which is dynamically adapted to the transient state of the system [16]. Thus, when compared to SET mechanisms, they have the potential to reduce unnecessary information transmissions and more effectively avoid the Zeno phenomenon in spacecraft formation [17]. Recent progress on DET mechanism-based multi-agent systems [16,18] and distributed SFF systems [15,19] has been reported. However, few results have focused on DET mechanism-based attitude synchronization control for SFF systems, which motivates this paper.

In addition, existing event-based attitude synchronization control approaches focus on reducing the communication trigger frequency, but the computational burden and synchronization control performance have not been well addressed. Applying these ETC techniques is challenging due to the limited computation resources on spaceborne computers. At present, adaptive radial basis function neural network (RBFNN)-based attitude synchronization control approaches have been developed for spacecraft formation, and the adaptive RBFNNs have been widely used in approximating the unknown nonlinear attitude dynamics [6], [7]. Compared to integral-based adaptive learning algorithms used in adaptive RBFNNs [6], [7], the algebraic P-type iterative learning algorithm requires less online computing power and is more robust to system disturbances or noises [20], [21]. Therefore, by combining a P-type iterative learning algorithm with neural network techniques, this paper aims to develop a DET mechanism and learning RBFNN-based robust attitude synchronization control for SFF systems.

In light of the aforementioned, this paper addresses the problem of learning RBFNN and DET mechanism-based robust attitude synchronization control of multi-spacecraft formation systems with limited communication, space disturbances, modeling uncertainties, and actuator faults. The main contributions of this paper are as follows:

1. To reduce communication frequency, we propose a DET mechanism that dynamically adjusts the trigger threshold. Compared with traditional SET mechanisms [10–14], the proposed DET mechanism has lower communication trigger numbers and more effectively avoids Zeno behavior.
2. A DET mechanism-based distributed self-learning neural-network control (SLN^{2}C) law is developed to guarantee the robust attitude synchronization of spacecraft formation. In the SLN^{2}C scheme, a learning RBFNN model is proposed to approximate and compensate for lumped disturbances online. Compared with traditional adaptive neural network control methods [6,7], the SLN^{2}C requires fewer computational resources while retaining the control accuracy of attitude synchronization.
3. A P-type iterative learning algorithm with variable learning intensity is adopted to update the weight matrix of the RBFNN model. Compared with the fixed learning intensity [20,21], the variable learning intensity can reduce the initial oscillation and weaken the saturation response [22,23].

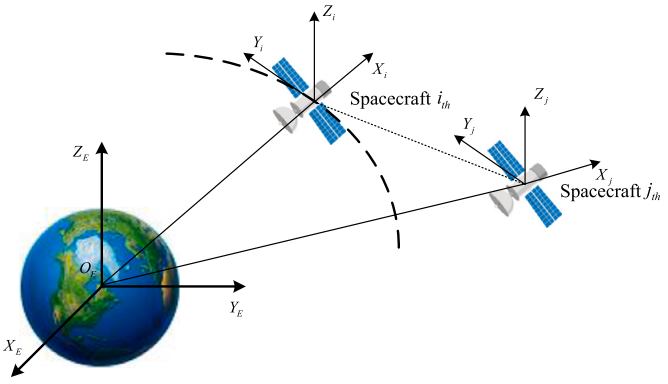

Fig. 1. Reference coordinate system used for spacecraft attitude control system modeling.

The remainder of this article is organized as follows: Section 2 illustrates the background and formulates the problem. Section 3 presents the DET mechanism-based SLN^{2}C design, stability analysis, and Zeno-free behavior analysis. A numerical simulation and comparison are given in Section 4. Finally, some concluding statements are provided in Section 5.

2. Background and problem formulation

2.1. Attitude control system modeling

The reference coordinate system used for spacecraft attitude control system modeling [24] is depicted in Fig. 1, where $F_E \triangleq \{O_E X_E Y_E Z_E\}$ represents the inertial coordinate system centered on the Earth, and $F_i \triangleq \{O_i X_i Y_i Z_i\}$ and $F_j \triangleq \{O_j X_j Y_j Z_j\}$ represent the body-fixed inertial coordinate system centered on the ith and jth spacecraft, respectively. Further, a rigid spacecraft is considered, and a unit quaternion is adopted to describe the spacecraft's attitude. The attitude kinematics and dynamics of the ith spacecraft [25] are modeled as follows:

$$\begin{bmatrix} \dot{q}_{i0} \\ \dot{\boldsymbol{q}}_i \end{bmatrix} = \begin{bmatrix} -\frac{1}{2}\boldsymbol{q}_i^{\mathrm{T}} \\ \frac{1}{2}(q_{i0}\boldsymbol{I}_3 + \boldsymbol{q}_i^{\times}) \end{bmatrix} \boldsymbol{\omega}_i \tag{1}$$

$$\boldsymbol{J}_{si}\dot{\boldsymbol{\omega}}_i + \boldsymbol{\omega}_i^{\times}\boldsymbol{J}_{si}\boldsymbol{\omega}_i = \boldsymbol{u}_i + \boldsymbol{p}_i \tag{2}$$

where for the ith spacecraft, $\boldsymbol{Q}_i = \frac{1}{2}(q_{i0}\boldsymbol{I}_3 + \boldsymbol{q}_i^{\times})$ is the attitude quaternion utilized to describe the spacecraft orientation of F_i w.r.t. F_E, and is expressed in F_i. Further, $\boldsymbol{q}_i^{\mathrm{T}}\boldsymbol{q}_i + q_{i0}^2 = 1$. $\boldsymbol{\omega}_i = \begin{bmatrix} \omega_{1i} & \omega_{2i} & \omega_{3i} \end{bmatrix}^{\mathrm{T}}$ represents the attitude angular velocity, $\boldsymbol{J}_{si} \in \mathbb{R}^{3\times 3}$ denotes the inertial matrix, $\boldsymbol{u}_i$ and $\boldsymbol{p}_i$ denote the control torque generated by actuators and the space environmental disturbance torque, respectively. Herein, $\boldsymbol{\omega}_i^{\times}$ represents

$$\boldsymbol{\omega}_i^{\times} = \begin{bmatrix} 0 & -\omega_{i3} & \omega_{i2} \\ \omega_{i3} & 0 & -\omega_{i1} \\ -\omega_{i2} & \omega_{i1} & 0 \end{bmatrix}$$

Considering the faults and distribution uncertainties in actuators, the actual actuator input [26] can be modeled as

$$\boldsymbol{u}_i = \boldsymbol{D}_{i1}\left[\boldsymbol{\Gamma}_i\boldsymbol{\tau}_i + \bar{\boldsymbol{\tau}}_i\right] \tag{3}$$

where $\boldsymbol{D}_{i1} = (\boldsymbol{D}_{i0} + \Delta\boldsymbol{D}_i) \in \mathbb{R}^{3\times m}$ denotes the actuator distribution matrix with $\boldsymbol{D}_{i0}$ being its nominal part and the uncertainty (or misalignment) part $\Delta\boldsymbol{D}_i$. The effectiveness matrix $\boldsymbol{\Gamma}_i = \mathrm{diag}\{\rho_{i1}, \cdots, \rho_{im}\}$ characterizes the health condition of the actuators with $\rho_{ij} \in (0, 1]$, $j \in [1, m]$,

and $\bar{\boldsymbol{\tau}}_i = (\bar{\tau}_{i1}, \cdots, \bar{\tau}_{im})^{\mathrm{T}}$ is the bias torque vector. Readers who are interested in actuator fault and actuator misalignment models can also refer to [27]. For the ith spacecraft, the inertia matrix $\boldsymbol{J}_{si} = \boldsymbol{J}_i + \Delta\boldsymbol{J}_i$ is assumed to have a nominal part $\boldsymbol{J}_i$ and an uncertainty part $\Delta\boldsymbol{J}_i$. Thus, when considering inertia uncertainties and actuator faults, the attitude dynamics (2) can be rewritten into

$$(\boldsymbol{J}_i + \Delta\boldsymbol{J}_i)\dot{\boldsymbol{\omega}}_i + \boldsymbol{\omega}_i^{\times}(\boldsymbol{J}_i + \Delta\boldsymbol{J}_i)\boldsymbol{\omega}_i = \boldsymbol{D}_{i1}\left[\boldsymbol{\Gamma}_i\boldsymbol{\tau}_i + \bar{\boldsymbol{\tau}}_i\right] + \boldsymbol{p}_i \tag{4}$$

Further, (4) can be transformed into

$$\boldsymbol{J}_i\dot{\boldsymbol{\omega}}_i + \boldsymbol{\omega}_i^{\times}\boldsymbol{J}_i\boldsymbol{\omega}_i = \boldsymbol{D}_{i1}\boldsymbol{\tau}_i + \boldsymbol{u}_{di} \tag{5}$$

where $\boldsymbol{u}_{di} = \boldsymbol{D}_{i1}((\boldsymbol{\Gamma}_i - \boldsymbol{I}_N)\boldsymbol{\tau}_i + \bar{\boldsymbol{\tau}}) + \Delta\boldsymbol{D}_i\boldsymbol{\tau}_i + \boldsymbol{p}_i + \Delta\boldsymbol{J}_i(\boldsymbol{\omega}_i)$ is the lumped disturbance, and $\Delta\boldsymbol{J}_i(\boldsymbol{\omega}_i) = -\Delta\boldsymbol{J}_i\dot{\boldsymbol{\omega}}_i - \boldsymbol{\omega}_i^{\times}\Delta\boldsymbol{J}_i\boldsymbol{\omega}_i$.

2.2. Attitude error dynamics

$(q_{id0}, \boldsymbol{q}_{id})$ is defined as the expected attitude quaternion, and $\boldsymbol{\omega}_{di}$ and $\dot{\boldsymbol{\omega}}_{di}$ as the expected attitude angular velocity and angular acceleration, respectively. Further, considering attitude tracking synchronization of spacecraft formation, for the ith spacecraft, the kinematics and dynamics of the attitude tracking errors [28] are described by

$$\begin{bmatrix}\dot{q}_{ie0}\\ \dot{\boldsymbol{q}}_{ie}\end{bmatrix} = \begin{bmatrix}-\frac{1}{2}\boldsymbol{q}_{ie}^{\mathrm{T}}\\ \boldsymbol{Q}(\boldsymbol{q}_{ie})\end{bmatrix}\boldsymbol{\omega}_{ie} \tag{6}$$

and

$$\begin{aligned}\boldsymbol{J}_i\dot{\boldsymbol{\omega}}_{ie} =& -\boldsymbol{\omega}_i^{\times}\boldsymbol{J}_i\boldsymbol{\omega}_i + \boldsymbol{J}_i(\boldsymbol{\omega}_{ie}^{\times}\boldsymbol{R}_{ie}\boldsymbol{\omega}_{di} - \boldsymbol{R}_{ie}\dot{\boldsymbol{\omega}}_{di})\\ &+ \boldsymbol{D}_{i1}\boldsymbol{\tau}_i + \boldsymbol{u}_{di}\end{aligned} \tag{7}$$

where $(q_{ie0}, \boldsymbol{q}_{ie})$ represents the attitude quaternion tracking error, $\boldsymbol{\omega}_{ie} = \boldsymbol{\omega}_i - \boldsymbol{R}_{ie}\boldsymbol{\omega}_{di}$ denotes angular velocity tracking error, and $\boldsymbol{R}_{ie}$ denotes the rotation matrix which can be described by

$$\boldsymbol{R}_{ie} = (q_{ie0}^2 - \boldsymbol{q}_{ie}^{\mathrm{T}}\boldsymbol{q}_{ie})\boldsymbol{I}_3 + 2\boldsymbol{q}_{ie}\boldsymbol{q}_{ie}^{\mathrm{T}} - 2q_{ie0}\boldsymbol{q}_{ie}^{\times} \tag{8}$$

2.3. Graph theory

A graph $G(\boldsymbol{A}) = \{\boldsymbol{V}, \boldsymbol{E}, \boldsymbol{A}\}$ is used to model the network topology among N spacecraft. The graph $G(\boldsymbol{A})$ consists of a finite spacecraft set $\boldsymbol{V} = \{1, \ldots, N\}$, a weighted adjacency matrix $\boldsymbol{A} = [a_{ij}]$, and an edge set $\boldsymbol{E} = \{(i,j) : i, j \in \boldsymbol{V}\}$, where $(i,j) \in \boldsymbol{E}$ implies that the jth spacecraft can obtain information from the ith spacecraft. For any $i, j \in \boldsymbol{V}, a_{ij} > 0$, if and only if $(i,j) \in \boldsymbol{E}$, whereas $a_{ij} = 0$ if and only if $(i,j) \notin \boldsymbol{E}$. The set of neighbors of the ith spacecraft is denoted by $n_i = \{j : (i,j) \in \boldsymbol{V}\}$. The Laplacian matrix $\boldsymbol{L} = [l_{ij}] = \boldsymbol{D} - \boldsymbol{A}$ with $\boldsymbol{D} = \mathrm{diag}(d_1, d_2, \ldots d_N)$, where $d_i = 1$ indicates that the ith spacecraft can obtain information from the leader spacecraft, and $d_i = 0$ otherwise. A graph is deemed to have a spanning tree if at least one spacecraft has a path (a sequence of edges in the form of $(i,j), (j,k), \cdots$) to all the other spacecraft.

Assumption 1. [29] The communication topology of the spacecraft formation is an undirected graph.

2.4. Problem formulation

The primary objective of this paper is to design a DET mechanism-based distributed SLN^{2}C law for robust attitude synchronization of a multiple SFF system with limited communication, space disturbances, modeling uncertainties, and actuator faults. Specifically, for any given reference attitude $\boldsymbol{q}_{di}$ and $\boldsymbol{\omega}_{di}$, we design a DET mechanism-based distributed SLN^{2}C law $\boldsymbol{\tau}_i$ for (6) and (7), such that the actual spacecraft attitude can synergistically track the expected attitude with an acceptable accuracy. In addition, it can guarantee a low communication trigger frequency and prevent the Zeno phenomenon under the DET mechanism-based distributed SLN^{2}C law.

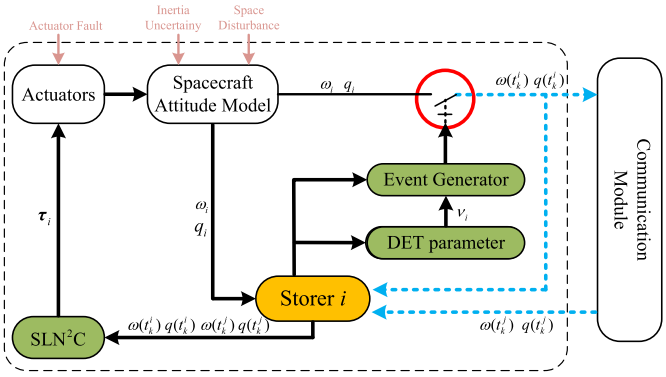

Fig. 2. Structure diagram of DET mechanism and SLN^{2}C-based spacecraft attitude synchronization control.

3. DET mechanism-based attitude synchronization control design

In this section, the SLN^{2}C law and the DET mechanism are respectively developed, and the stability analysis of the DET mechanism-based SLN^{2}C law is detailed. Further, we analyze the Zeno phenomenon avoidance under the DET mechanism-based SLN^{2}C law. The structure diagram of the DET mechanism and SLN^{2}C-based spacecraft attitude synchronization control is illustrated in Fig. 2.

3.1. Neural network estimation review

Firstly, we briefly review the RBFNN-based unknown nonlinear dynamics approximation method. For any continuous function $\boldsymbol{f}(\boldsymbol{x}) : \mathbb{R}^n \to \mathbb{R}^m$ with $\boldsymbol{f}(\boldsymbol{0}) = [0\ 0\ 0]^{\mathrm{T}}$ with $\boldsymbol{x} \in \mathbb{R}^n$ belongs to a compact set $\boldsymbol{\Lambda}_x$, there exists an ideal weight matrix $\boldsymbol{M} \in \mathbb{R}^{m\times p}$, such that

$$\boldsymbol{f}(\boldsymbol{x}) = \boldsymbol{M}^{\mathrm{T}}\boldsymbol{h}(\boldsymbol{x}) + \varepsilon \tag{9}$$

where $\boldsymbol{M}$ is a weight matrix and ε is the bounded approximation error. $\boldsymbol{h}(\boldsymbol{x}) = [h_1(\boldsymbol{x}), h_2(\boldsymbol{x}), \cdots h_p(\boldsymbol{x})]^{\mathrm{T}} \in \mathbb{R}^{\mathrm{p}}$ is a radial basis function, where the ith element is defined by

$$h_i(\boldsymbol{x}) = \exp\left(-\frac{\|\boldsymbol{x} - \boldsymbol{c}_i\|_2^2}{2B_i^2}\right) \tag{10}$$

where $\boldsymbol{c}_i \in \mathbb{R}^n$ represents the center of the receptive field and B_i represents the width of the Gaussian function. $\|\cdot\|$ is the Euclidean norm for a vector. Therefore, an ideal optimal weight $\boldsymbol{M}^*$ exists s.t. the error can be minimized for all $\boldsymbol{x} \in \boldsymbol{\Lambda}_x$, i.e.

$$\boldsymbol{M}^* = \arg\min_{\boldsymbol{M}\in\mathbb{R}^{m\times p}}\left\{\sup_{x\in\boldsymbol{\Lambda}_x}\left\|\boldsymbol{f}(\boldsymbol{x}) - \boldsymbol{M}^{\mathrm{T}}h(\boldsymbol{x})\right\|\right\} \tag{11}$$

Remark 1. In existing RBFNN-based spacecraft attitude synchronization control methods [6], [7], adaptive RBFNN models are used to approximate unknown nonlinear attitude dynamics, and various adaptive algorithms have been developed to update the unknown weight matrix $\hat{\boldsymbol{M}}$. Considering the advantages of a P-type iterative learning algorithm [20], [21], a learning RBFNN model will be investigated in the later section.

3.2. Event-based self-learning neural-network control law

For attitude synchronization control, we define two total errors in attitude quaternion and attitude angular velocity as

$$\boldsymbol{x}_{i1} = d_i\boldsymbol{q}_{ie} + \sum_{j=1, j\neq i}^{N} a_{ij}(\boldsymbol{q}_{ie} - \boldsymbol{q}_{je}) \tag{12}$$

$$= d_i\boldsymbol{q}_{ie} + \sum_{j=1, j\neq i}^{N} l_{ij}\boldsymbol{q}_{ie}, \tag{13}$$

$$\boldsymbol{x}_{i2} = d_i\boldsymbol{\omega}_{ie} + \sum_{j=1,j\neq i}^{N} a_{ij}(\boldsymbol{\omega}_{ie} - \boldsymbol{\omega}_{je}) \tag{14}$$

$$= d_i\boldsymbol{\omega}_{ie} + \sum_{j=1,j\neq i}^{N} l_{ij}\boldsymbol{\omega}_{ie} \tag{15}$$

where d_i, a_{ij}, and l_{ij} represent the corresponding elements of $\boldsymbol{D}$, $\boldsymbol{A}$, and $\boldsymbol{L}$, respectively. $\boldsymbol{\omega}_{je}$ represents the attitude angular velocity of the jth spacecraft w.r.t. the frame F_i, and

$$\boldsymbol{\omega}_{je} = \boldsymbol{R}_{ij}\boldsymbol{\omega}_{je}^{j} \tag{16}$$

where $\boldsymbol{\omega}_{je}^{j}$ denotes the angular velocity of jth spacecraft w.r.t. the frame F_j, the rotation matrix $\boldsymbol{R}_{ij}$ is given by

$$\boldsymbol{R}_{ij} = (q_{ij0}^2 - \boldsymbol{q}_{ij}^{\mathrm{T}}\boldsymbol{q}_{ij})\boldsymbol{I}_3 + 2\boldsymbol{q}_{ij}\boldsymbol{q}_{ij}^{\mathrm{T}} - 2q_{ij0}\boldsymbol{q}_{ij}^{\times} \tag{17}$$

with $q_{ij0} = q_{ie0} - q_{je0}$ and $\boldsymbol{q}_{ij} = \boldsymbol{q}_{ie} - \boldsymbol{q}_{je}$. Then, (12) and (14) can be rewritten as

$$\boldsymbol{x}_1 = \boldsymbol{H}\boldsymbol{q}_e, \tag{18}$$

$$\boldsymbol{x}_2 = \boldsymbol{H}\boldsymbol{\omega}_e \tag{19}$$

where $\boldsymbol{q}_e = [\boldsymbol{q}_{1e}, \boldsymbol{q}_{2e}, \ldots, \boldsymbol{q}_{ne}]^{\mathrm{T}}$, $\boldsymbol{\omega}_e = [\boldsymbol{\omega}_{1e}, \boldsymbol{\omega}_{2e}, \ldots, \boldsymbol{\omega}_{ne}]^{\mathrm{T}}$, $\boldsymbol{x}_1 = [\boldsymbol{x}_{11}, \boldsymbol{x}_{21}, \ldots, \boldsymbol{x}_{n1}]^{\mathrm{T}}$, $\boldsymbol{x}_2 = [\boldsymbol{x}_{12}, \boldsymbol{x}_{22}, \ldots, \boldsymbol{x}_{n2}]^{\mathrm{T}}$, and $\boldsymbol{H}$ is a positive definite symmetric matrix, which is defined as $\boldsymbol{H} = (\boldsymbol{L} + \boldsymbol{D}) \otimes \boldsymbol{I}_3$.

An auxiliary variable is further defined as

$$\boldsymbol{S} = \boldsymbol{K}_1\boldsymbol{x}_1 + \boldsymbol{x}_2 \tag{20}$$

where $\boldsymbol{S} = [\boldsymbol{s}_1, \boldsymbol{s}_2, \ldots, \boldsymbol{s}_n]^{\mathrm{T}}$ and $\boldsymbol{K}_1 = \mathrm{diag}(k_1, \ldots, k_1)$ with constants $k_1 > 0$. Therefore, substituting (18) and (19) into (20) yields

$$\boldsymbol{S} = \boldsymbol{K}_1\boldsymbol{H}\boldsymbol{q}_e + \boldsymbol{H}\boldsymbol{\omega}_e \tag{21}$$

To guarantee robust and accurate attitude synchronization control, a learning RBFNN model is designed to approximate and compensate for the lumped disturbance $\boldsymbol{u}_{di}$, and its structure is as follows:

$$\hat{\boldsymbol{u}}_{di} = \hat{\boldsymbol{M}}_i(t)\boldsymbol{h}(\boldsymbol{s}_i), \tag{22}$$

$$\hat{\boldsymbol{M}}_i(t) = \theta_i\hat{\boldsymbol{M}}_i(t-\tau) + \boldsymbol{K}_{si}\boldsymbol{s}_i\boldsymbol{h}_i^{\mathrm{T}}(\boldsymbol{s}_i) \tag{23}$$

with variable learning intensity

$$\theta_i = \exp(-\gamma_1(\|\hat{\boldsymbol{M}}_i(t-\tau)\| + \varsigma)^{\gamma_2}) \tag{24}$$

where $\boldsymbol{K}_{si} \in \mathbb{R}^{3\times3}$, $\gamma_1 > 0$, $\gamma_2 > 0$, and $\varsigma > 0$.

An SLN^{2}C law is designed for (7) based on the learning RBFNN model (22) as follows,

$$\boldsymbol{\tau}_i(t) = \boldsymbol{D}_{i1}^{\circ}\boldsymbol{J}_i\left(-\boldsymbol{N}_i(t) - k_2\boldsymbol{s}_i(t) - k_3\tanh(\boldsymbol{s}_i(t)) - \hat{\boldsymbol{u}}_{di}\right) \tag{25}$$

where $k_2 > 0$ and $k_3 > 0$. $\boldsymbol{D}_{i1}^{\circ}$ denotes the pseudo-inverse matrix of $\boldsymbol{D}_{i1}$, i.e., $\boldsymbol{D}_{i1}^{\circ} = \boldsymbol{D}_{i1}^{\mathrm{T}}(\boldsymbol{D}_{i1}\boldsymbol{D}_{i1}^{\mathrm{T}})^{-1}$. $\boldsymbol{N}_i(t)$ is defined as

$$\boldsymbol{N}_i(t) = k_1\dot{\boldsymbol{q}}_{ie} - \boldsymbol{J}_i^{-1}\boldsymbol{\omega}_i^{\times}\boldsymbol{J}_i\boldsymbol{\omega}_i + (\boldsymbol{\omega}_{ie}^{\times}\boldsymbol{R}_{ie}\boldsymbol{\omega}_d - \boldsymbol{R}_{ie}\dot{\boldsymbol{\omega}}_d). \tag{26}$$

Denote the sampling value of $\boldsymbol{s}_i(t)$ as

$$\hat{\boldsymbol{s}}_i(t) = \boldsymbol{s}_i(t_k^i) \quad \text{for} \quad t \in [t_k^i, t_{(k+1)}^i) \tag{27}$$

where t_k^i formulates a time sequence. An event-based SLN^{2}C law is constructed based on (25) as follows:

$$\boldsymbol{\tau}_i(t_k^i) = \boldsymbol{D}_{i1}^{\circ}\boldsymbol{J}_i\left(-\boldsymbol{N}_i(t_k^i) - k_2\boldsymbol{s}_i(t_k^i) - k_3\tanh(\boldsymbol{s}_i(t_k^i)) - \widehat{\boldsymbol{u}}_{di}\right) \tag{28}$$

Based on (22) and (23), the sampling value of $\hat{\boldsymbol{u}}_{di}$ at the latest event time instant is updated using $\widehat{\boldsymbol{u}}_{di}$,

$$\widehat{\boldsymbol{u}}_{di} = \widehat{\boldsymbol{M}}_i(t)\boldsymbol{h}_i(\hat{\boldsymbol{s}}_i), \tag{29}$$

with

$$\widehat{\boldsymbol{M}}_i(t) = \theta_i\widehat{\boldsymbol{M}}_i(t-\tau) + \boldsymbol{K}_{si}\hat{\boldsymbol{s}}_i\boldsymbol{h}_i^{\mathrm{T}}(\hat{\boldsymbol{s}}_i) \tag{30}$$

Remark 2. From (24), it can be noted that θ_i is monotonically decreasing with respect to $\widehat{\boldsymbol{M}}_i(t-\tau)$. In addition, ς can guarantee that $\theta_i \neq 1$ when $\widehat{\boldsymbol{M}}_i(t-\tau) = 0$, and $\theta_i \to 0$ only when $\widehat{\boldsymbol{M}}_i(t-\tau) \to \infty$; thus, $\theta_i \in (0, 1)$. In (24), γ_1 denotes the decay rate away from 0, γ_2 determines the flatness degree of θ_i near 0, and ς guarantees that $\theta_i < 1$. The learning intensity θ_i decays fast when a large γ_1 is chosen, and is flat when a large γ_2 is chosen. In addition, (23) reveals that θ_i is strengthened when $\boldsymbol{s}_i$ approaches the stable state and is weakened when $\boldsymbol{s}_i$ becomes large.

Remark 3. In (22), a learning RBFNN model is adopted to approximate the lumped disturbance $\boldsymbol{u}_{di}$, in which a P-type iterative learning algorithm with a variable learning intensity is used to update the weight matrix of the RBFNN model. The primary property of the variable learning intensity is that the learning RBFNN model (22) could adaptively and smoothly approximate the lumped disturbance $\boldsymbol{u}_{di}$. Compared to the fixed learning intensity [20,21], the variable learning intensity can reduce the initial oscillation and weaken the saturation response due to its adaptability and smoothing abilities [22,23], but requires more computational resources due to the adaptive updating law (24).

Remark 4. In [20], a P-type iterative learning algorithm is proposed to approximate the lumped disturbance $\boldsymbol{u}_{di}$, assuming that the indirect increment of $\boldsymbol{u}_{di}$ is norm-bounded. In the existing adaptive RBFNN models [6], [7], the weight constraint that $||\hat{\boldsymbol{M}}(t)||_\infty \leq d$ with a positive constant d is usually required. In this paper, the learning RBFNN model (22) has no restrictions on the lumped disturbance $\boldsymbol{u}_{di}$ when a high approximation accuracy is required. Therefore, the proposed learning RBFNN model provides a wider range of applications than current approaches [6,7,20].

To obtain the main results, the following lemmas are given.

Lemma 1. *[22] The variable learning intensity (24) implies*

$$\exp(-\gamma_1(M_{i\max} + \varsigma)^{\gamma_2}) < \theta_i(t) < \exp(-\gamma_1\varsigma^{\gamma_2}) < 1 \tag{31}$$

Lemma 2. *[30] Given two matrices $\boldsymbol{X}$ and $\boldsymbol{Z}$ with approximate dimensions, a positive definite symmetric matrix $\boldsymbol{H}$ exists such that*

$$\boldsymbol{X}^T\boldsymbol{Z} + \boldsymbol{Z}^T\boldsymbol{X} \leq \boldsymbol{X}^T\boldsymbol{H}\boldsymbol{Z} + \boldsymbol{Z}^T\boldsymbol{H}^{-1}\boldsymbol{X} \tag{32}$$

Lemma 3. *[31] For the vector $\chi = [\chi_1^T, \ldots, \chi_n^T]^T \in \mathbb{R}^{N\times n}$, where $\chi_i \in \mathbb{R}^N, i = 1, \ldots n$, one has*

$$0 \leq \tanh^T(\chi)\tanh(\chi) \leq \chi^T\tanh(\chi) \tag{33}$$

3.3. Dynamic event-triggered mechanism design

To achieve the conversion between $\boldsymbol{s}_i(t_k^i)$ and $\boldsymbol{s}_i(t)$, the following variables are defined:

$$\bar{s}_i = k_1(\boldsymbol{q}_{ie} + \sum_{j=1,j\neq i}^{N} a_{ij}(\boldsymbol{q}_{ie} - \boldsymbol{q}_{je}(t_k^j))) + \boldsymbol{\omega}_{ie} + \sum_{j=1,j\neq i}^{N} a_{ij}(\boldsymbol{\omega}_{ie} - \boldsymbol{\omega}_{je}(t_k^j)) \tag{34}$$

$$\boldsymbol{v}_{i1} = \boldsymbol{q}_{ie}(t_k^i) - \boldsymbol{q}_{ie}(t) \tag{35}$$

$$\boldsymbol{v}_{i2} = \boldsymbol{\omega}_{ie}(t_k^i) - \boldsymbol{\omega}_{ie}(t) \tag{36}$$

$$\boldsymbol{\zeta}_i = \boldsymbol{N}_i(t_k^i) - \boldsymbol{N}_i(t) \tag{37}$$

and

$$\boldsymbol{\eta}_i = \hat{\boldsymbol{u}}_{di} - \widehat{\boldsymbol{u}}_{di}. \tag{38}$$

Let $\boldsymbol{e}_i = \hat{\boldsymbol{s}}_i - \bar{\boldsymbol{s}}_i$, and define the following error as

$$\begin{aligned}\boldsymbol{\xi}_i &= \hat{\boldsymbol{s}}_i - \boldsymbol{s}_i \\ &= \boldsymbol{e}_i - k_1 \sum_{j=1, j\neq i}^{N} a_{ij}\boldsymbol{\upsilon}_{i1} - \sum_{j=1, j\neq i}^{N} a_{ij}\boldsymbol{\upsilon}_{i2}\end{aligned} \tag{39}$$

To further reduce unnecessary communication triggers resulting from a static triggering condition with a constant threshold [12], the dynamic triggering condition is then designed as

$$\begin{cases} t_{k+1} = \inf\{t > t_k : \delta_i(t) > 0\} \\ \delta_i(t) = \vartheta_i(\|\boldsymbol{\zeta}_i\| + \|\boldsymbol{\xi}_i\| + \|\boldsymbol{s}_i\| \left\|\boldsymbol{J}_i^{-1}\boldsymbol{\eta}_i\right\| - \iota_i) - \nu_i(t) \end{cases} \tag{40}$$

where $\iota_i = k_4^2 \exp(\frac{1}{2}(1 + k_5 \tanh(\|\hat{\boldsymbol{s}}_i\|)))$ and $\vartheta_i > 0$. Further, a dynamic variable $\nu_i(t)$ is introduced as

$$\dot{\nu}_i(t) = -\chi_i \nu_i(t) + \mu_i(-\|\boldsymbol{\zeta}_i\| - \|\boldsymbol{\xi}_i\| - \|\boldsymbol{s}_i\| \|\boldsymbol{J}_i^{-1}\boldsymbol{\eta}_i\| + \iota_i) \tag{41}$$

where $\nu_i(0) > 0$, $\chi_i > 0$, and $\mu_i > 0$. For each interval $t \in [t_k^i, t_{(k+1)}^i)$, (40) can be rewritten as follows:

$$\|\boldsymbol{\zeta}_i\| + \|\boldsymbol{\xi}_i\| + \|\boldsymbol{s}_i\| \left\|\boldsymbol{J}_i^{-1}\boldsymbol{\eta}_i\right\| - \iota_i > \frac{1}{\vartheta_i}\nu_i(t) \tag{42}$$

Further, substituting (41) into (42) leads to

$$\dot{\nu}_i > -\chi_i \nu_i + \frac{1}{\vartheta_i}\nu_i \tag{43}$$

From (43), it is trivial to verify that

$$\nu_i(t) > 0 \tag{44}$$

Remark 5. The DET mechanism (40) is designed such that the executive trigger is dynamically updated and adjusted based on the real-time sampling error. Specifically, if the sampling error exceeds the expected threshold value specified in (41), the auxiliary variable $\boldsymbol{s}_i$ will be updated and transmitted to adjacent spacecraft. Therefore, the proposed DET mechanism can better reduce the communication trigger frequency during attitude maneuvering.

Remark 6. The DET mechanism (40) reveals that a low communication trigger frequency can be obtained if χ_i is selected to be large. Intuitively, this will sacrifice the attitude convergence accuracy. The parameter ϑ_i has an opposite effect on χ_i. A simulation comparison of the DET mechanism with different χ_i and ϑ_i values will be provided in detail.

3.4. Stability analysis of DET mechanism-based attitude synchronization control law

Theorem 1. *For the attitude tracking error kinematics (6) and dynamics (7), if the gain parameters of the designed SLN^{2}C law (25) and of the DET mechanism (40) satisfy*

$$\frac{1}{2}\sigma_2 - \mu \leq 0 \tag{45}$$

$$\mu - \lambda_{Q\max} \leq 0 \tag{46}$$

$$\lambda_{Q\max}\boldsymbol{J}_i^{-1} - \alpha_3 \boldsymbol{K}_{si}^T = 0 \tag{47}$$

$$\alpha_3 \theta_i^2 (1 + \varpi) - 1 \leq 0 \tag{48}$$

where $\sigma_2 = 1 + k_2 + 2b_1 k_3$ with $b_1 > 0$ and $k_2 > 1$, $\alpha_3 > 0$, $\varpi > 0$, and $\lambda_{Q\max}$ is the largest eigenvalue of matrix $\boldsymbol{PH}$ with positive-definite symmetric matrix $\boldsymbol{P} \in \mathbb{R}^{3\times 3}$. The following stability results can be obtained,

1. *The value of the auxiliary variable $\boldsymbol{s}_i(t)$ is bounded, i.e., there exists a positive small constant Δ_1 such that the constraint $\lim_{t\to\infty} \|\boldsymbol{s}_i(t)\| \leq \Delta_1$ is satisfied.*
2. *The attitude angular velocity error $\boldsymbol{\omega}_e$ and attitude quaternion error $\boldsymbol{q}_e$ respectively satisfy constraints $\lim_{t\to\infty} \|\boldsymbol{\omega}_{ie}\| \leq \Delta_2$ and $\lim_{t\to\infty} \|\boldsymbol{q}_{ie}\| \leq \Delta_3$, where Δ_2 and Δ_3 are positive small constants.*
3. *The attitude synchronization control errors satisfy constraints $\lim_{t\to\infty} \|\boldsymbol{\omega}_{ie} - \boldsymbol{\omega}_{je}\| \leq \Delta_4$ and $\lim_{t\to\infty} \|\boldsymbol{q}_{ie} - \boldsymbol{q}_{je}\| \leq \Delta_5$, where Δ_4 and Δ_5 are positive small constants.*

Proof. An energy function candidate is considered as follows

$$V = V_1 + V_2 + V_3 \tag{49}$$

where $V_1 = \frac{1}{2}\boldsymbol{S}^{\mathrm{T}}\boldsymbol{P}\boldsymbol{S}$, $V_2 = \sum_{i=1}^{N} \nu_i(t)$, and

$$V_3 = \sum_{i=1}^{N} \int_{t-\tau}^{t} tr(\tilde{\boldsymbol{M}}_i^{\mathrm{T}}(t)\tilde{\boldsymbol{M}}_i(t))\mathrm{d}t$$

with $\tilde{\boldsymbol{M}}_i(t) = \boldsymbol{M}_i(t) - \hat{\boldsymbol{M}}_i(t)$. First, the approximation error dynamics of the lumped disturbance $\boldsymbol{u}_{di}(t)$ is given by

$$\tilde{\boldsymbol{u}}_{di}(t) = \boldsymbol{u}_{di}(t) - \hat{\boldsymbol{u}}_{di}(t) = \tilde{\boldsymbol{M}}_i(t)\boldsymbol{h}_i(\boldsymbol{s}_i) \tag{50}$$

where

$$\tilde{\boldsymbol{M}}_i(t) = \theta_i \tilde{\boldsymbol{M}}_i(t-\tau) - \boldsymbol{K}_{si}\boldsymbol{s}_i\boldsymbol{h}_i^{\mathrm{T}}(\boldsymbol{s}_i) + \Delta\boldsymbol{M}_i(t) \tag{51}$$

with $\Delta\boldsymbol{M}_i(t) = \boldsymbol{M}_i(t) - \theta_i\boldsymbol{M}_i(t-\tau)$. Then, the derivative of the Lyapunov function (49) can be obtained as

$$\begin{aligned}\dot{V} =& \dot{V}_1 + \dot{V}_2 + \dot{V}_3 \\ =& \boldsymbol{S}^T\boldsymbol{P}\dot{\boldsymbol{S}} + \sum_{i=1}^{N}\dot{\nu}_i(t) + \sum_{i=1}^{N}\Big\{-\alpha_2 tr(\tilde{\boldsymbol{M}}_i^{\mathrm{T}}(t)\boldsymbol{M}_i(t)) \\ & -tr(\tilde{\boldsymbol{M}}_i^{\mathrm{T}}(t-\tau)\boldsymbol{M}_i(t-\tau)) + \alpha_3 tr(\tilde{\boldsymbol{M}}_i^{\mathrm{T}}(t)\boldsymbol{M}_i(t))\Big\}\end{aligned} \tag{52}$$

where $\alpha_3 = 1 + \alpha_2$ with $\alpha_2 > 0$.

Further, substituting (21) into (52) yields

$$\begin{aligned}\dot{V}_1 &= \boldsymbol{S}^{\mathrm{T}}\boldsymbol{Q}(-k_2\hat{\boldsymbol{s}}_i + \boldsymbol{N}_i - \boldsymbol{N}_i(t_{ki}^i) - k_3\tanh(\hat{\boldsymbol{s}}_i) + \boldsymbol{J}_i^{-1}\boldsymbol{u}_{di} - \boldsymbol{J}_i^{-1}\widehat{\boldsymbol{u}}_{di}) \\ &\leq \lambda_{Q\max}(\sum_{i=1}^{V} -\frac{1}{2}k_2\boldsymbol{s}_i^{\mathrm{T}}\hat{\boldsymbol{s}}_i - \frac{1}{2}k_2\boldsymbol{s}_i^{\mathrm{T}}\hat{\boldsymbol{s}}_i + \boldsymbol{s}_i^{\mathrm{T}}(\boldsymbol{N}_i - \boldsymbol{N}_i(t_{ki}^i)) \\ &\quad - k_3\boldsymbol{s}_i^{\mathrm{T}}\tanh(\hat{\boldsymbol{s}}_i)) + \lambda_{Q\max}\sum_{i=1}^{N}\boldsymbol{s}_i^{\mathrm{T}}\boldsymbol{J}_i^{-1}(\boldsymbol{u}_{di} - \widehat{\boldsymbol{u}}_{di}) \\ &= dV_{11} + dV_{12}\end{aligned} \tag{53}$$

where

$$\begin{aligned}dV_{11} = \lambda_{Q\max}(&\sum_{i=1}^{N} -\frac{1}{2}k_2\boldsymbol{s}_i^{\mathrm{T}}\hat{\boldsymbol{s}}_i - \frac{1}{2}k_2\boldsymbol{s}_i^{\mathrm{T}}\hat{\boldsymbol{s}}_i \\ &+ \boldsymbol{s}_i^{\mathrm{T}}(\boldsymbol{N}_i - \boldsymbol{N}_i(t_{ki}^i)) - k_3\boldsymbol{s}_i^{\mathrm{T}}\tanh(\hat{\boldsymbol{s}}_i))\end{aligned} \tag{54}$$

and

$$dV_{12} = \lambda_{Q\max}\sum_{i=1}^{N}\boldsymbol{s}_i^{\mathrm{T}}\boldsymbol{J}_i^{-1}(\boldsymbol{u}_{di} - \widehat{\boldsymbol{u}}_{di}). \tag{55}$$

Combining (37) and (39), dV_{11} in (53) yields

$$\begin{aligned}dV_{11} = \frac{1}{2}(&-\sum_{i=1}^{N}k_2\|\boldsymbol{s}_i\|^2 - \sum_{i=1}^{N}k_2\|\hat{\boldsymbol{s}}_i\|^2 + \sum_{i=1}^{N}k_2\|\boldsymbol{\xi}_i\|^2) \\ &+ \sum_{i=1}^{N}\|\hat{\boldsymbol{s}}_i\|\|\boldsymbol{\zeta}_i\| - \sum_{i=1}^{N}\boldsymbol{\xi}_i^{\mathrm{T}}\boldsymbol{\zeta}_i - \sum_{i=1}^{N}k_3\boldsymbol{s}_i^{\mathrm{T}}\tanh(\hat{\boldsymbol{s}}_i)\end{aligned} \tag{56}$$

According to Lemma 2, one has

$$-\sum_{i=1}^{N}\xi_i^{\mathrm{T}}\zeta_i \le \sum_{i=1}^{N}\|\xi_i\|\,\|\zeta_i\| \le \frac{1}{2}\Big(\sum_{i=1}^{N}\|\zeta_i\|^2+\sum_{i=1}^{N}\|\xi_i\|^2\Big), \tag{57}$$

and

$$\sum_{i=1}^{N}\|\hat{s}_i\|\,\|\zeta_i\| \le \frac{1}{2}\Big(\sum_{i=1}^{N}\|\hat{s}_i\|^2+\sum_{i=1}^{N}\|\zeta_i\|^2\Big) \tag{58}$$

Following Lemma 3,

$$\begin{aligned}\sum_{i=1}^{N}k_3 s_i^{\mathrm{T}}\tanh(\hat{s}_i) &= \sum_{i=1}^{N}k_3\hat{s}_i^{\mathrm{T}}\tanh(\hat{s}_i)-\sum_{i=1}^{N}k_3\xi_i\tanh(\hat{s}_i)\\ &\le \sum_{i=1}^{N}k_3\tanh^{\mathrm{T}}(\hat{s}_i)\tanh(\hat{s}_i)+\sum_{i=1}^{N}k_3\xi_i\tanh(\hat{s}_i)\\ &\le \sum_{i=1}^{N}k_3\,\|\tanh(\hat{s}_i)\|+b_1k_3\sum_{i=1}^{N}\|\xi_i\|+\frac{1}{4b_1}k_3\end{aligned} \tag{59}$$

Combining (57)-(59), (56) can be simplified into

$$\begin{aligned}dV_{11} \le & -\frac{1}{2}\sum_{i=1}^{N}k_2\|s_i\|^2-\frac{1}{2}\sum_{i=1}^{N}k_2\|\hat{s}_i\|^2+\frac{1}{2}\sum_{i=1}^{N}k_2\|\xi_i\|^2+\frac{1}{2}\sum_{i=1}^{N}\|\hat{s}_i\|^2\\ &+\frac{1}{2}\sum_{i=1}^{N}\|\zeta_i\|^2+\frac{1}{2}\sum_{i=1}^{N}\|\xi_i\|^2-\sum_{i=1}^{N}k_3\,\|\tanh(\hat{s}_i)\|\\ &+\frac{1}{2}\sum_{i=1}^{N}\|\zeta_i\|^2+b_1k_3\sum_{i=1}^{N}\|\xi_i\|^2+\frac{1}{4b_1}k_3\\ \le & \frac{1}{2}(-k_2+1)\sum_{i=1}^{N}\|\hat{s}_i\|^2+\frac{1}{2}(k_2+1+b_1k_3)\sum_{i=1}^{N}\|\xi_i\|^2\\ &-\frac{1}{2}\sum_{i=1}^{N}k_2\|s_i\|^2-\sum_{i=1}^{N}k_3\,\|\tanh(\hat{s}_i)\|+\frac{1}{4b_1}k_3+\sum_{i=1}^{N}\|\zeta_i\|^2\end{aligned} \tag{60}$$

Let $\sigma_2 = 1+k_2+2b_1k_3$; (53) can be rewritten as

$$\begin{aligned}\dot{V}_1 \le & \sum_{i=1}^{N}\frac{1}{2}\sigma_1\|\hat{s}_i\|^2+\frac{1}{2}\sigma_2\big(\|\xi_i\|^2+\|\zeta_i\|^2\big)+dV_{12}\\ &+\lambda_{Q\max}\Big(-\frac{1}{2}\sum_{i=1}^{N}k_2\|s_i\|^2-\sum_{i=1}^{N}k_3\,\|\tanh(\hat{s}_i)\|+\frac{1}{4b_1}k_3\Big)\end{aligned} \tag{61}$$

Combining (38), dV_{12} can be transformed into

$$\begin{aligned}dV_{12} &= \lambda_{Q\max}\sum_{i=1}^{N}s_i^{\mathrm{T}}J_i^{-1}(u_{di}-\widehat{u}_{di})\\ &= \lambda_{Q\max}\sum_{i=1}^{N}s_i^{\mathrm{T}}J_i^{-1}(u_{di}-\hat{u}_{di}+\eta_i)\\ &\le \lambda_{Q\max}\sum_{i=1}^{N}s_i^{\mathrm{T}}J_i^{-1}(\tilde{M}_i(t)h(s_i))+\lambda_{Q\max}\sum_{i=1}^{N}\big\|s_i^{\mathrm{T}}\big\|\,\big\|J_i^{-1}\eta_i\big\|\end{aligned} \tag{62}$$

From (62), one obtains

$$\begin{aligned}dV_{12}+\dot{V}_3 = & \sum_{i=1}^{N}-\alpha_2 tr(\tilde{M}_i(t)M_i(t))+\sum_{i=1}^{N}\alpha_3 tr(\theta_i^2\tilde{M}_i^{\mathrm{T}}(t-\tau)\tilde{M}_i^{\mathrm{T}}(t-\tau))\\ &+\sum_{i=1}^{N}2\theta_i s_i^{\mathrm{T}}(\lambda_{Q\max}J_i^{-1}-\alpha_3K_{si}^{\mathrm{T}})\tilde{M}_i(t-\tau)h(s_i)\\ &+\sum_{i=1}^{N}2s_i^{\mathrm{T}}(\lambda_{Q\max}J_i^{-1}-\alpha_3K_{si}^{\mathrm{T}})\Delta M_i(t)h(s_i)\\ &+\sum_{i=1}^{N}s_i^{\mathrm{T}}(\lambda_{Q\max}J_i^{-1}-2\alpha_3K_{si}^{\mathrm{T}})K_{si}s_ih^{\mathrm{T}}(s_i)h(s_i)\\ &+\sum_{i=1}^{N}2\theta_i\tilde{M}_i^{\mathrm{T}}(t-\tau)\Delta M_i(t)+\sum_{i=1}^{N}\Delta M_i^{\mathrm{T}}(t)\Delta M_i(t)\\ &-tr(\tilde{M}_i^{\mathrm{T}}(t-\tau)\tilde{M}_i^{\mathrm{T}}(t-\tau))+\lambda_{Q\max}\sum_{i=1}^{N}\big\|s_i^{\mathrm{T}}\big\|J_i^{-1}\eta_i\end{aligned} \tag{63}$$

Under condition (47) in *Theorem* 1, (63) can be simplified as

$$\begin{aligned}dV_{12}+\dot{V}_3 \le & -\sum_{i=1}^{N}\alpha_2 tr(\tilde{M}_i^{\mathrm{T}}(t)M_i(t))+\lambda_{Q\max}\sum_{i=1}^{N}\big\|s_i^{\mathrm{T}}\big\|\,\big\|J_i^{-1}\eta_i\big\|\\ &+\sum_{i=1}^{N}\alpha_3 tr(\theta_i^2\tilde{M}_i^{\mathrm{T}}(t-\tau)\tilde{M}_i^{\mathrm{T}}(t-\tau)+\Delta M_i^{\mathrm{T}}(t)\Delta M_i(t))\\ &+\sum_{i=1}^{N}\alpha_3(2\theta_i\tilde{M}_i^{\mathrm{T}}(t-\tau)\Delta M_i(t)-tr(\tilde{M}_i^{\mathrm{T}}(t-\tau)\tilde{M}_i(t-\tau)))\\ &-\sum_{i=1}^{N}\alpha_3 s_i^{\mathrm{T}}K_{si}^{\mathrm{T}}K_{si}s_ih^{\mathrm{T}}(s_i)h(s_i)\end{aligned} \tag{64}$$

From Lemma 2, the following inequality holds,

$$\begin{aligned}&2\theta_i tr(\tilde{M}_i^{\mathrm{T}}(t-\tau)\Delta M_i(t))\\ &\le \theta_i^2\varpi tr(\tilde{M}_i^{\mathrm{T}}(t-\tau)(\tilde{M}_i(t-\tau))+\frac{1}{\varpi}tr(\Delta M_i^{\mathrm{T}}(t)\Delta M_i(t))\end{aligned} \tag{65}$$

where $\varpi > 0$. Therefore, considering (61) and substituting (65) into (64), we have

$$\begin{aligned}\dot{V}_1+\dot{V}_3 \le & \frac{1}{2}\sigma_1\sum_{i=1}^{N}\|\hat{s}_i\|^2+\frac{1}{2}\sigma_2\sum_{i=1}^{N}\big(\|\xi_i\|^2+\|\zeta_i\|^2\big)\\ &+\lambda_{Q\max}\Big(-\frac{1}{2}\sum_{i=1}^{N}k_2\|s_i\|^2-\sum_{i=1}^{N}k_3\,\|\tanh(\hat{s}_i)\|+\frac{1}{4b_1}k_3\Big)\\ &+\sum_{i=1}^{N}\alpha_3\theta_i^2((1+\varpi)-1)tr(\tilde{M}_i^{\mathrm{T}}(t-\tau)\tilde{M}_i(t-\tau))\\ &-\sum_{i=1}^{N}\alpha_2 tr(\tilde{M}_i(t)M_i(t))+\lambda_{Q\max}\sum_{i=1}^{N}\|s_i\|\,\big\|J_i^{-1}\eta_i\big\|\\ &+\sum_{i=1}^{N}\alpha_3(1+\frac{1}{\varpi})tr(\Delta M_i^{\mathrm{T}}(t)\Delta M_i(t))\end{aligned} \tag{66}$$

Based on the trigger condition (41), $\dot{V}_2$ is

$$\dot{V}_2 = \sum_{i=1}^{N}-\chi_i\nu_i(t)+\mu(-\|\zeta_i\|-\|\xi_i\|-\|s_i\|\,\big\|J_i^{-1}\eta_i\big\|+\iota_i)) \tag{67}$$

Combined with (66) and (67), $\dot{V}$ can be obtained as

$$\begin{aligned}\dot{V} \le & \frac{1}{2}\sigma_1\sum_{i=1}^{N}\|\hat{s}_i\|^2+(\frac{1}{2}\sigma_2-\mu)\sum_{i=1}^{N}\big(\|\xi_i\|^2+\|\zeta_i\|^2\big)-\chi_i\nu_i(t)\\ &+(\mu-\lambda_{Q\max})\sum_{i=1}^{N}\big\|s_i^{\mathrm{T}}\big\|\,\big\|J_i^{-1}\eta_i\big\|-\sum_{i=1}^{N}\alpha_2 tr(\tilde{M}_i(t)M_i(t))\\ &+\sum_{i=1}^{N}\alpha_3(1+\frac{1}{\varpi})tr(\Delta M_i^{\mathrm{T}}(t)\Delta M_i(t))+\iota_i+\lambda_{Q\max}\frac{1}{4b_1}k_3\\ &-\frac{1}{2}\lambda_{Q\max}\sum_{i=1}^{N}k_3\,\|\tanh(\hat{s}_i)\|-\frac{1}{2}\lambda_{Q\max}\sum_{i=1}^{N}k_2\|s_i\|^2\end{aligned} \tag{68}$$

where $\tanh(\cdot)$ is a hyperbolic tangent function, which means that $\tanh(\chi_i)\in[-1,1]$, $\forall\chi_i\in\mathbb{R}^n, i=1,\dots n$. If condition (44) holds, (68) can be simplified as

$$\begin{aligned}\dot{V} \le & \sum_{i=1}^{N}-\frac{1}{2}\lambda_{Q\max}k_2\|s_i\|^2+\lambda_{Q\max}\frac{1}{4b_1}k_3\\ &+\alpha_3(1+\frac{1}{\varpi})tr(\Delta M_i^{\mathrm{T}}(t)\Delta M_i(t))+\iota_i\end{aligned} \tag{69}$$

where ι_i is bounded, and $\Delta \boldsymbol{M}_i(t)$ is a small value. From (69), it can be seen that $\dot{V}$ is bounded, which indicates $\boldsymbol{s}_i$ is convergent. In other words, $\|\boldsymbol{\omega}_{ei}\|$ and $\|\boldsymbol{q}_{ie}\|$ are bounded, and $\|\boldsymbol{\omega}_{ie}-\boldsymbol{\omega}_{je}\|$ and $\|\boldsymbol{q}_{ie}-\boldsymbol{q}_{je}\|$ are bounded. This completes the proof of Theorem 1. ■

Corollary 1. *For the attitude tracking error kinematics (6) and dynamics (7), if the designed SLN^{2}C law (25) with the fixed learning intensity θ_i and DET mechanism (40) satisfy constraints (45)-(48), then 1-3 in Theorem 1 hold.*

Remark 7. Corollary 1 reveals that the designed DET mechanism-based SLN^{2}C law with the fixed learning intensity can still ensure the stability of the closed-loop system despite sacrificing the initial dynamic performance and the saturation performance. In Corollary 1, the P-type iterative learning algorithm with the variable learning intensity will be degraded into the traditional P-type iterative learning algorithms [20], [21]. Compared with the learning RBFNN model with the variable learning intensity, the learning RBFNN model with the fixed learning intensity has a simpler structure and requires fewer computation resources. In addition, compared with adaptive RBFNN models [6], [7], the learning RBFNN model with the fixed learning intensity has less computation consumption because the P-type iterative learning algorithm has this advantage over the integral-based adaptive learning algorithm.

3.5. Zeno behavior analysis

Theorem 2. *Considering the DET mechanism (40) designed for the attitude tracking error kinematics (6) and dynamics (7), if two consecutive triggering intervals satisfy that $t_{k+1}-t_k>\Delta_6$ with a constant value Δ_6, then the DET mechanism-based SLN^{2}C law can guarantee that spacecraft attitude synchronization control exhibits no Zeno behavior.*

Proof. If $k_c \geq \|\boldsymbol{s}_i\|\,\|\boldsymbol{J}_i^{-1}\|$, the DET mechanism (40) satisfies

$$0<\|\boldsymbol{\zeta}_i\|+\|\boldsymbol{\xi}_i\|+\|\boldsymbol{s}_i\|\left\|\boldsymbol{J}_i^{-1}\boldsymbol{\eta}_i\right\|-\iota_i \tag{70}$$

From *Theorem* 1, $\boldsymbol{s}_i$, $\boldsymbol{N}_i$, and $\hat{\boldsymbol{u}}_{di}$ are all bounded. Therefore, positive constants k_u, k_N, and k_s exist such that $\|\hat{\boldsymbol{u}}_{di}\|\leq k_u$, $\|\boldsymbol{N}_i\|\leq k_N$ and $\|\boldsymbol{s}_i\|\leq k_s$. According to the DET mechanism (40), $h_i(t)$ is defined as

$$\begin{aligned}
h_i(t)&=\|\boldsymbol{\zeta}_i\|+\|\boldsymbol{\xi}_i\|+k_c\|\boldsymbol{\eta}_i\|\\
&=\int_{t_k}^{t_{k+1}}\left\|\dot{\boldsymbol{N}}_i(t_{ki}^i)-\dot{\boldsymbol{N}}_i(t)\right\|dt\\
&\quad+\int_{t_k}^{t_{k+1}}\left\|\dot{\hat{\boldsymbol{s}}}_i-\dot{\boldsymbol{s}}_i\right\|dt+k_c\int_{t_k}^{t_{k+1}}\left\|\dot{\hat{\boldsymbol{u}}}_{di}-\dot{\widehat{\boldsymbol{u}}}_{di}\right\|dt\\
&=k_c\int_{t_k}^{t_{k+1}}\|\dot{\hat{\boldsymbol{u}}}_{di}\|dt+\int_{t_k}^{t_{k+1}}\|-\dot{\boldsymbol{N}}_i(t)\|dt+\int_{t_k}^{t_{k+1}}\|-\dot{\boldsymbol{s}}_i\|dt\\
&\leq(k_ck_u+k_N+k_s)(t_{k+1}-t_k)
\end{aligned} \tag{71}$$

From (71), one obtains

$$t_{k+1}-t_k\geq\frac{\iota_i}{(k_ck_u+k_N+k_s)} \tag{72}$$

Therefore, from (72), the interval deviation between two trigger intervals is strictly greater than a positive scalar, implying Zeno behavior can be effectively avoided by applying the DET mechanism-based SLN^{2}C law. This completes the proof. ■

Remark 8. In Theorem 2, the avoidance of the Zeno behavior is analyzed. Evidently, a strictly positive trigger interval can be guaranteed under the discontinuous DET mechanism-based SLN^{2}C law. Therefore, a DET mechanism-based SLN^{2}C law can effectively avoid Zeno phenomenon. In practical application, this trigger interval should not be less than the sampling interval of a spacecraft on-board computer.

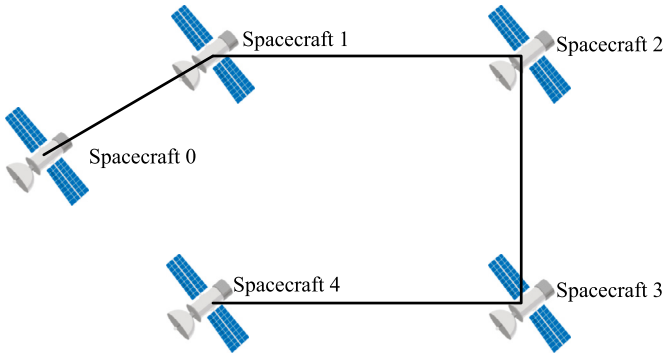

Fig. 3. Communication topology of a spacecraft formation flying system.

Remark 9. Based on the static triggering condition [12], we introduce a dynamic triggering condition with a dynamic variable $\nu_i(t)$. Note that the dynamic triggering condition will be degraded into the static triggering condition if $\nu_i(t)=0$. From (40), it can be found that the proposed dynamic trigger mechanism allows a larger time interval between adjacent triggers than the static triggering mechanism when $\nu_i(t)>0$. Therefore, the proposed dynamic trigger mechanism is more effective in avoiding Zeno behavior. In addition, the detailed theoretical comparison between the above two event-triggered mechanisms on the avoidance of Zeno behavior can be found in [32].

4. Numerical simulation

We provide a numerical example to verify the effectiveness and superiority of the proposed control method.

4.1. Simulation setting

As depicted in Fig. 3, an SFF system including a leader spacecraft (Spacecraft 0) and four follower spacecraft (Spacecraft 1-4) [12] is considered in the simulation. From the communication topology provided in Fig. 3, the adjacency matrix $\boldsymbol{A}$ can be assumed as,

$$\boldsymbol{A}=\begin{bmatrix}0&0.01&0&0\\0.01&0&0.01&0\\0&0.01&0&0.01\\0&0&0.01&0\end{bmatrix}.$$

Further, the inertia matrices of four follower spacecraft are

$$\boldsymbol{J}_1=\begin{bmatrix}20&0&0.9\\0&17&0\\0&0.9&15\end{bmatrix},\boldsymbol{J}_2=\begin{bmatrix}21&0&0.8\\0&17&0\\0.8&0&14\end{bmatrix},$$

$$\boldsymbol{J}_3=\begin{bmatrix}23&0&0.9\\0&19&0.2\\0.9&0.2&17\end{bmatrix},\boldsymbol{J}_4=\begin{bmatrix}23&0&0.9\\0&19&0.2\\0.9&0.2&17\end{bmatrix},$$

and the inertia uncertainties are $\Delta\boldsymbol{J}_i=\mathrm{diag}(6,7,8)e^{-10t}-\mathrm{diag}(1,1,1)l(t)+\mathrm{diag}(\sin(0.5t),\cos(0.5t),\sin(0.5t))$ where $l(t)$ is a step function,

$$l(t)=\begin{cases}0 & t<10\ \mathrm{s}\\ 1 & t\geq 10\ \mathrm{s}\end{cases}$$

Six actuators are equipped in each of the four follower spacecraft with a maximum output torque of 0.5 Nm. The actuator distribution matrix [33] and its uncertainty are, respectively, considered as

Table 1
Values of initial and expected attitude for spacecraft formation.

Parameters	Values
Initial attitude quaternion	$q_1(0) = [\sqrt{1/3} \quad 0 \quad -\sqrt{1/3} \quad \sqrt{1/3}]^{\mathrm{T}}$ $q_2(0) = [0.7 \quad 0 \quad -0.1 \quad 0.5]^{\mathrm{T}}$ $q_3(0) = [\sqrt{0.4} \quad 0.1 \quad -\sqrt{0.29} \quad \sqrt{0.3}]^{\mathrm{T}}$ $q_3(0) = [0.3 \quad \sqrt{0.35} \quad 0 \quad \sqrt{0.4}]^{\mathrm{T}}$
Initial attitude angular velocity	$\boldsymbol{\omega}_i(0) = [0 \quad 0 \quad 0]^{\mathrm{T}}$
Expected attitude angular velocity	$\boldsymbol{\omega}_{di} = [0.1\sin(0.01t) \quad -0.1\sin(0.01t) \quad 0.1\sin(0.001t)]^{\mathrm{T}}$
Expected attitude quaternion	$\boldsymbol{q}_{di} = [1 \quad 0 \quad 0 \quad 0]^{\mathrm{T}}$

Table 2
Parameters of the SLN^{2}C and DET mechanism.

Terms	Value
SLN^{2}C law	$k_1 = 0.5$, $k_2 = 1.1$, $k_3 = 0.1$, $\varsigma = 0.01$, $B_i = 2$, $\boldsymbol{K}_{si} = \mathrm{diag}(0.9, 0.9, 0.9)$, $\gamma_1 = 2$, $\gamma_2 = 4$, $\boldsymbol{c}_i = \begin{bmatrix} -0.8 & -0.8 & -0.8 \\ 0 & 0 & 0 \\ 4.5 & 4.5 & 4.5 \end{bmatrix}$
DET mechanism	$k_4 = 0.001$, $k_5 = 10$, $\chi_i = 1$, $\mu = 1.5$, $\vartheta_i = 0.3$, $b_1 = 1$

$$\boldsymbol{D}_{i1} = \begin{bmatrix} 0.8 & -0.8 & 0 & 0 & 0 & 0 \\ 0 & 0 & 0.7 & -0.7 & 0 & 0 \\ 0 & 0 & 0 & 0 & 0.7 & -0.7 \end{bmatrix}$$

and $\Delta \boldsymbol{D}_i = 0.05\boldsymbol{D}_{i1} + 0.01\mathrm{rand}(3, 6)$. The effectiveness matrix $\boldsymbol{\Gamma}$ is set to be

$$\rho_j = 0.8 + 0.05\mathrm{rand}_{\Delta t} + 0.05\sin(0.4t + j\pi/3)$$

where $j = 1, \ldots 6$, and the bias torque is $\bar{\tau}_i = 0.1[1, 2, 3, 2, 1, 3]$ Nm. The space disturbances are

$$\boldsymbol{p}_1 = 0.1[0.1\sin(\pi t/20) \; 0.15\cos(\pi t/25) \; 0.2\sin(\pi t/30)]^{\mathrm{T}}$$

$$\boldsymbol{p}_2 = 0.1[0.1\sin(\pi t/20) \; 0.13\cos(\pi t/25) \; 0.5\sin(\pi t/30)]^{\mathrm{T}}$$

$$\boldsymbol{p}_3 = 0.1[0.1\cos(\pi t/20) \; 0.15\sin(\pi t/25) \; 0.17\cos(\pi t/30)]^{\mathrm{T}}$$

$$\boldsymbol{p}_4 = 0.1[0.1\cos(\pi t/20) \; 0.13\sin(\pi t/25) \; 0.15\cos(\pi t/30)]^{\mathrm{T}}$$

The initial and expected attitude values for spacecraft formation are given in Table 1. Parameters of the SLN^{2}C law and DET mechanism from Section 3 are listed in Table 2.

4.2. Simulation evaluation analysis

The tracking errors of attitude angular velocity and attitude quaternion under the designed DET mechanism-based SLN^{2}C law are shown in Fig. 4 and Fig. 5, respectively. Both figures show that the attitude and angular velocity errors accurately converge to the neighborhood of the zero region. Fig. 6 shows the curves of the learning intensity in the learning RBFNN model, whereas Fig. 7 illustrates the actuator output control torques under variable learning intensity (Fig. 7a) and a fixed constant learning intensity (Fig. 7b), respectively. Fig. 6 shows that the adapted learning intensities change within the range of (0, 1). In addition, Fig. 7 reveals that, compared with the fixed learning intensity, actuator saturation can be effectively attenuated under the variable learning intensity.

To further illustrate the superiority of the variable learning intensity, we compare the energy consumption between two types of learning intensities. The energy cost index function [34] is defined as $\boldsymbol{E} = \frac{1}{2}\int_0^{\mathrm{T}} \|\boldsymbol{u}_i\| \, \mathrm{dt}$, where T denotes the simulation time. The energy con-

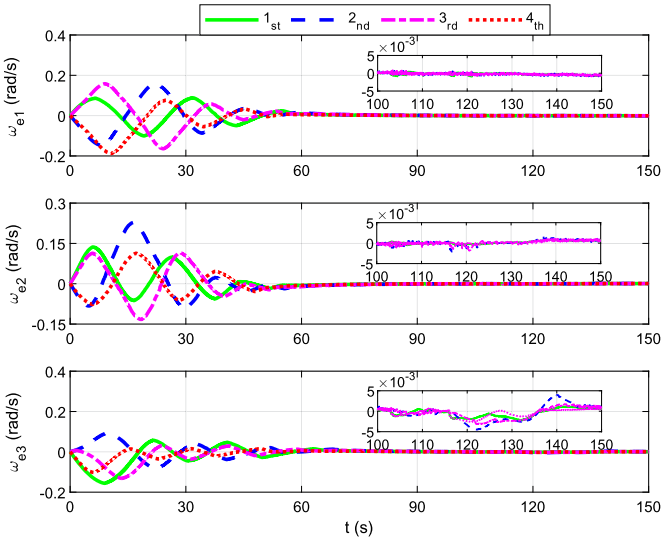

Fig. 4. Tracking error curves of attitude angular velocity for spacecraft formation.

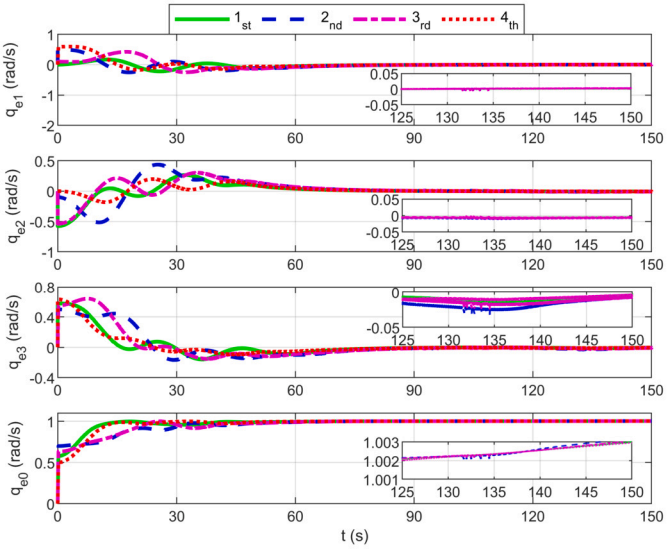

Fig. 5. Tracking error curves of attitude quaternion for spacecraft formation.

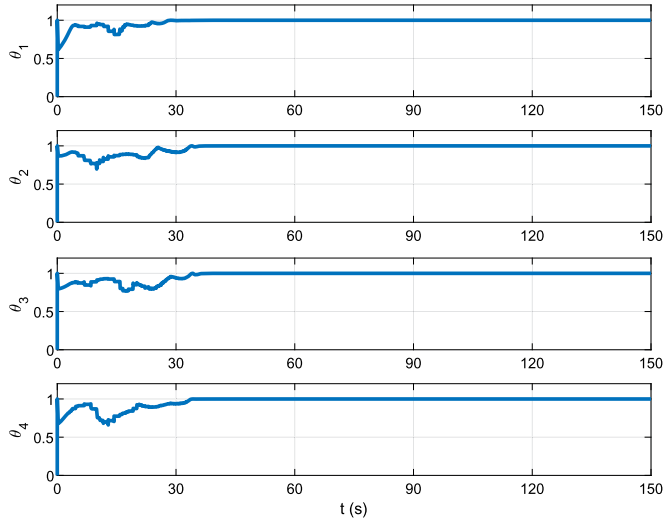

Fig. 6. Curves of variable learning intensity $\theta_i, i = 1, 2, 3, 4$.

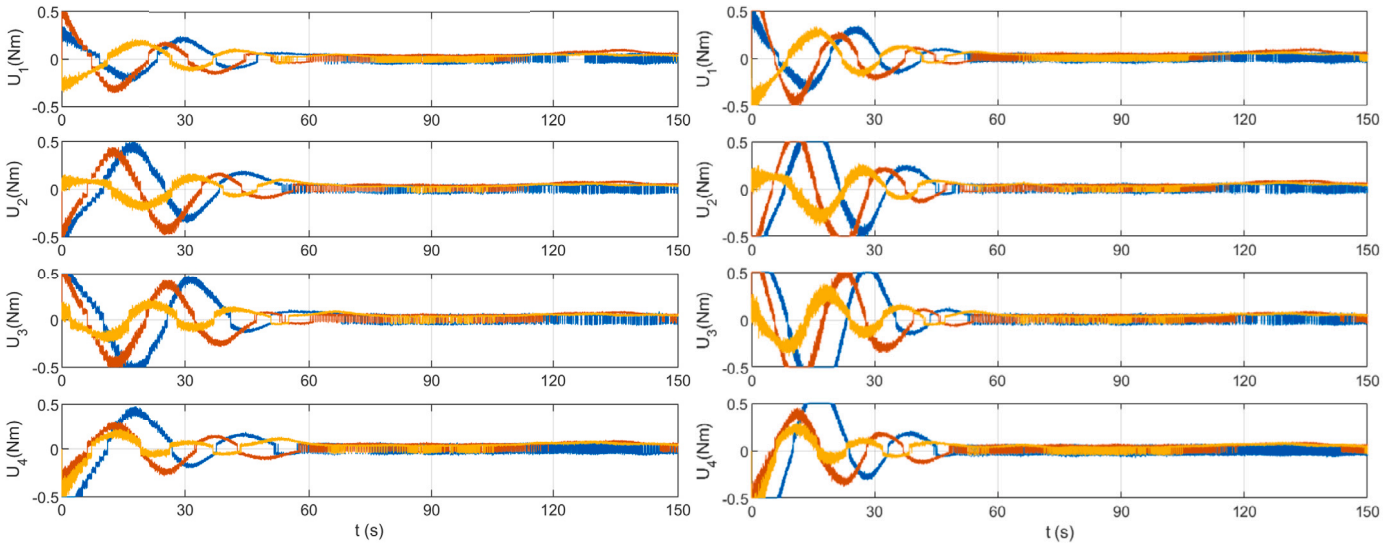

a. Variable θ_i in (24) b. Fixed $\theta_i = 0.98$

Fig. 7. Curves of control torques under the variable and fixed learning intensity.

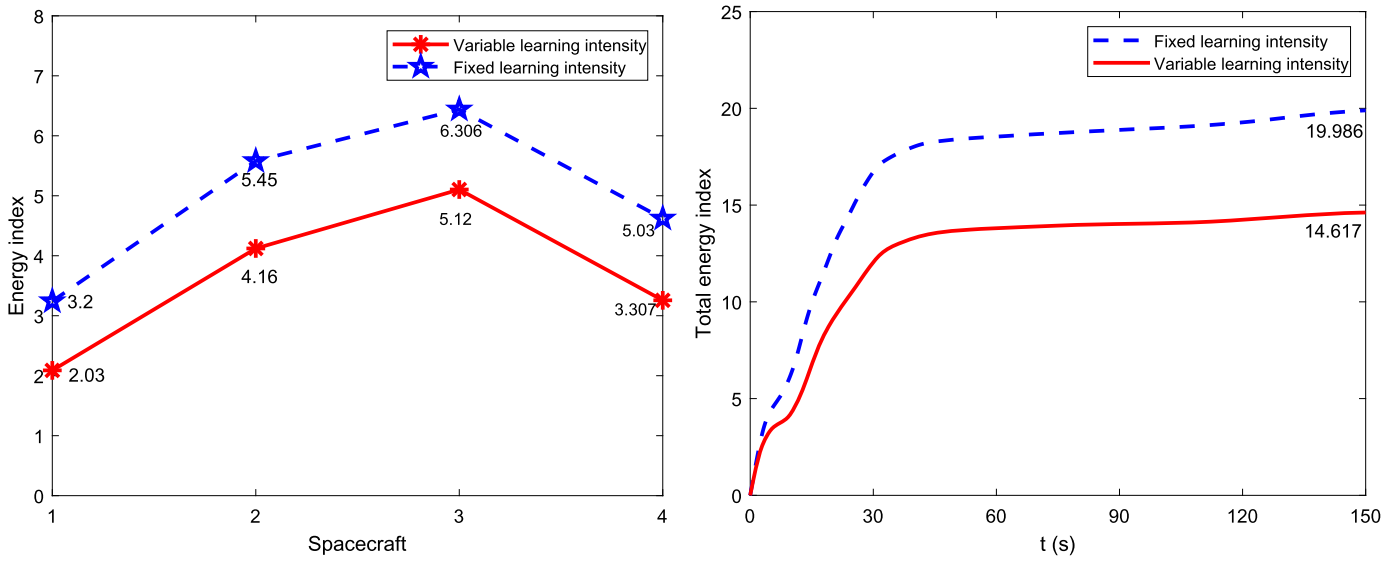

a.Single energy consumption b.Total energy consumption

Fig. 8. Comparison of energy consumption between the variable and fixed learning intensity.

sumption of the single spacecraft and all spacecraft under two different learning intensities are shown in Fig. 8. Noticeably, compared with the fixed learning intensity, the designed variable learning intensity has lower energy consumption in attitude synchronization control.

Further, the trigger instants and intervals of four spacecraft under the DET mechanism-based SLN^{2}C law are shown in Fig. 9, and the communication frequencies of four spacecraft are analyzed in Table 3. Fig. 9 shows that frequent information interactions among neighboring spacecraft are not required in the proposed DET mechanism, which is also verified by the lower and upper bounds on time intervals between two successive triggering instants in Table 3. In addition, the minimum trigger interval of all four follower spacecraft is 0.1 s, which is greater than the 0.05 s sampling step. This indicates the absence of Zeno behavior for attitude synchronization control under the DET mechanism-based SLN^{2}C law.

In the DET mechanism-based SLN^{2}C law design, parameters χ_i and ϑ_i have an important influence on the communication trigger number and attitude synchronization control performance. Therefore, the time responses of the communication trigger frequency under different values of χ_i and ϑ_i are illustrated in Fig. 10. Fig. 11 depicts the attitude quaternion tracking errors of all four spacecraft. Fig. 10 shows that a large χ_i results in lower communication trigger numbers and attitude tracking accuracy. Notably, compared with parameter χ_i, parameter ϑ_i has the opposite effect on communication trigger number and attitude tracking accuracy. Therefore, a trade-off between the communication

Table 3
Communication frequency analysis of four spacecraft.

Spacecraft	1_{st}	2_{nd}	3_{rd}	4_{th}
Total number	1130	1105	1119	1139
Max interval (s)	5.9	5.6	5.6	5.7
Min interval (s)	0.1	0.1	0.1	0.1
Reduction rate	96.23%	96.32%	96.27%	96.20%

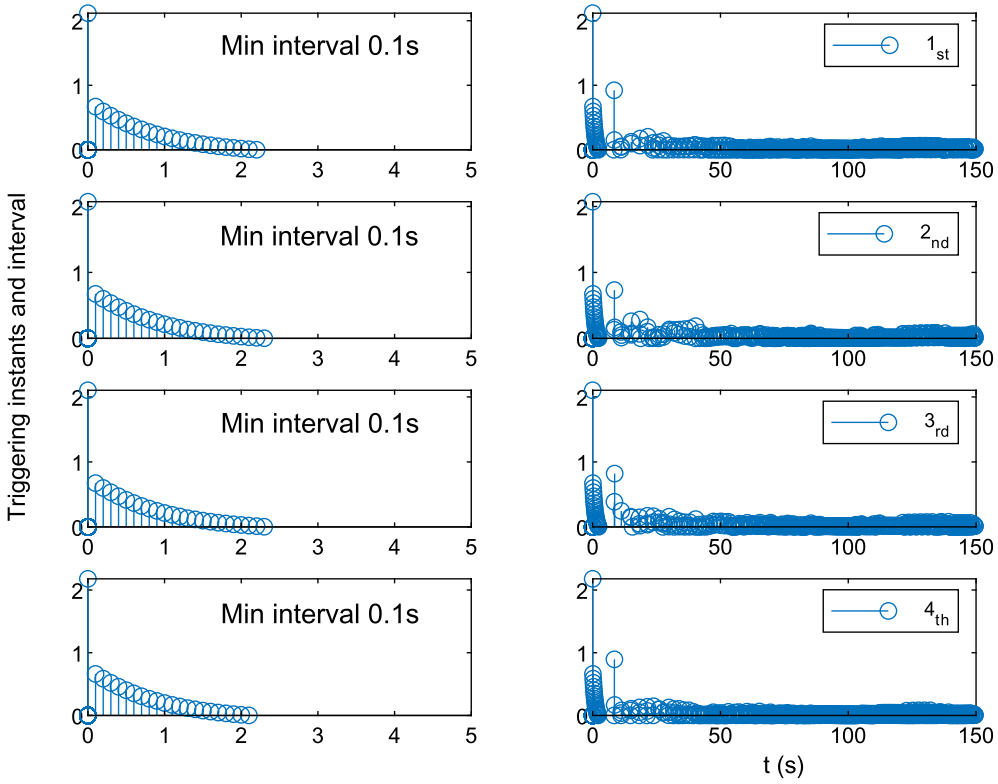

Fig. 9. Triggering instants and interval of four spacecraft.

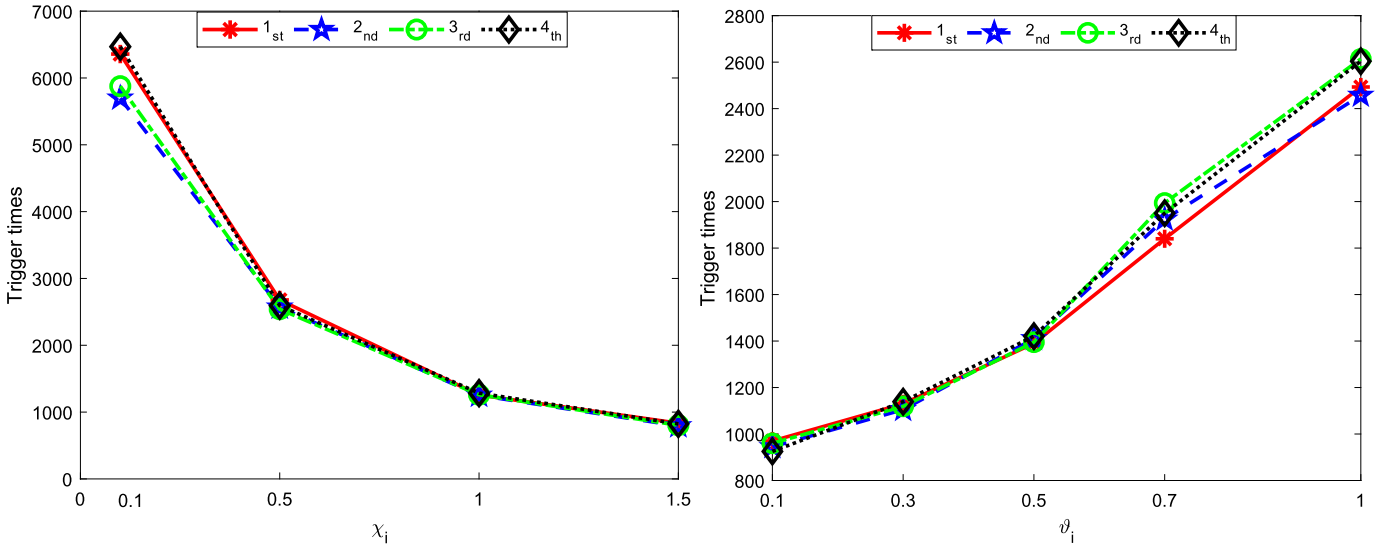

a. values of χ_i b. values of ϑ_i

Fig. 10. Trigger numbers generated by four follower spacecraft when considering different values of χ_i and ϑ_i.

trigger frequency and attitude synchronization control performance should be made in practical applications.

4.3. Performance comparison

To illustrate the superiority of the proposed event-based attitude synchronization control method, a simulation comparison between the DET mechanism-based SLN^{2}C law, a DET mechanism-based control method [12] (Example 1 for short), and a SET mechanism-based control method [14] (Example 2 for short) was performed.

Table 4
Comparison results of the attitude quaternion error.

Terms	SLN^{2}C	Example 1 [12]	Example 2 [14]
q_{e0}	0.003	0.02	0.005
q_{e1}	0.01	0.1	0.04
q_{e2}	0.01	0.05	0.04
q_{e3}	0.05	0.1	0.1

Comparison results of the above two event-based attitude synchronization control methods are provided in Fig. 12, Fig. 13, and Table 4.

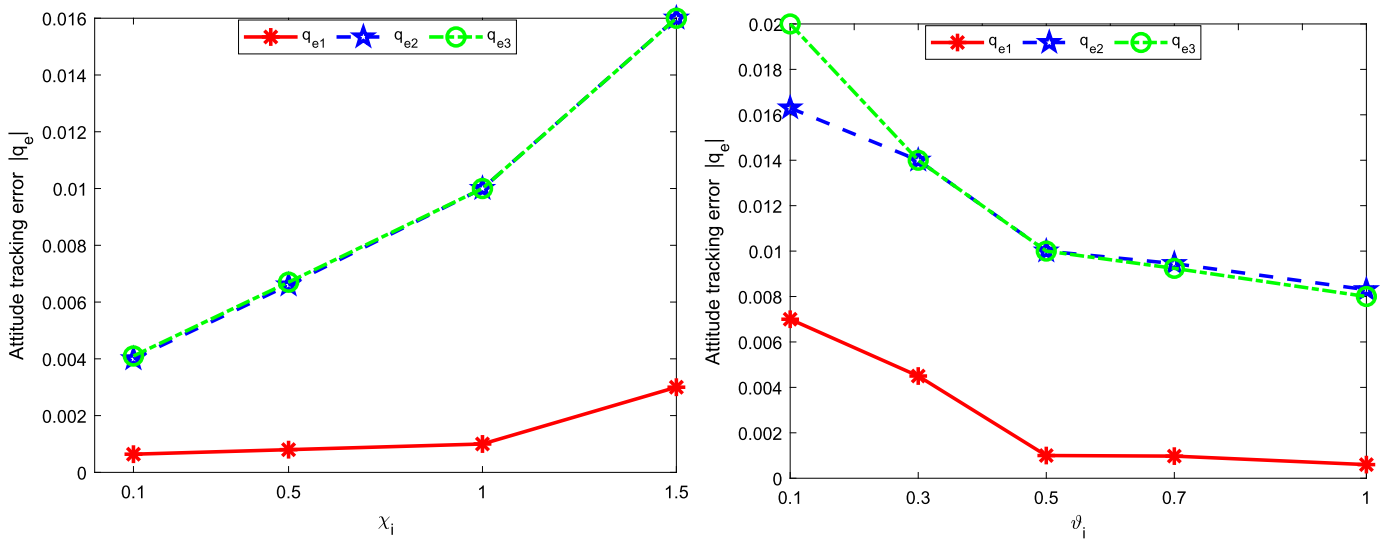

a. values of χ_i b. values of ϑ_i

Fig. 11. Tracking error curves of attitude quaternion for four follower spacecraft when considering different values of χ_i and ϑ_i.

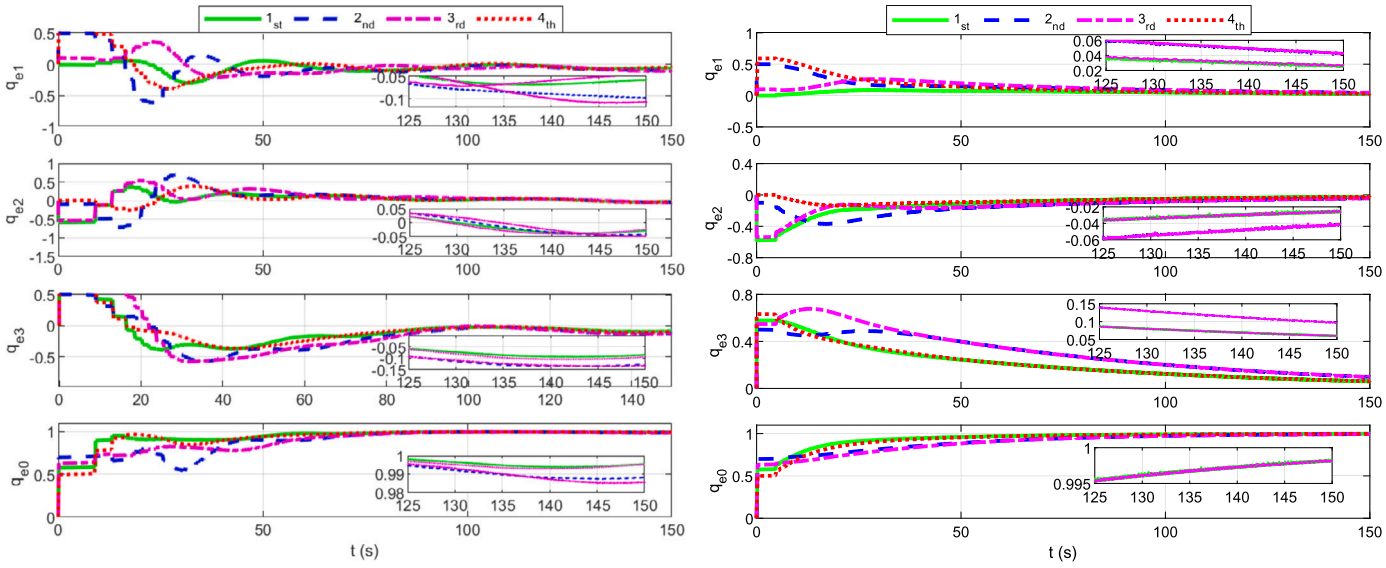

a. Example 1 b. Example 2

Fig. 12. Tracking error curves of attitude quaternion for spacecraft formation in Example 1 [12] and Example 2 [14].

Fig. 12(a) and Fig. 12(b) depict the tracking error curves of attitude quaternion for spacecraft formation in Examples 1 and 2, respectively. Fig. 12 shows that the event-based distributed control methods proposed in [12] and [14] can also achieve attitude synchronization control of multi-spacecraft formation. Fig. 13(a) and Fig. 13(b) provide the trigger instants and intervals of four follower spacecraft in Example 1 and Example 2, respectively.

Further, the communication trigger numbers under the above three synchronization control methods are computed and illustrated in Fig. 14. Noticeably, the proposed DET mechanism-based SLN^{2}C method has lower communication trigger numbers than event-based synchronization control methods in Examples 1 and 2. In other words, the proposed DET mechanism-based SLN^{2}C method requires less communication resources. In addition, Table 4 illustrates that, under the influence of disturbance, inertia, and actuator faults, the DET mechanism-based SLN^{2}C method achieves better attitude synchronization control performance. Consequently, the DET mechanism-based SLN^{2}C method can not only reduce the communication frequency, but also ensure the synchronization control accuracy of the SFF system.

5. Concluding remarks

This paper investigates the issue of robust attitude synchronization of spacecraft formation with limited communication under the DET mechanism-based SLN^{2}C design. The DET mechanism has been developed to reduce the communication trigger frequency via a dynamic trigger threshold. Further, the DET mechanism-based SLN^{2}C law has been designed such that it can not only achieve robust attitude synchronization control but also guarantee a low communication frequency and avoid Zeno behavior effectively. In the proposed SLN^{2}C law, the learning RBFNN model has been utilized to approximate the lumped disturbance and a variable learning intensity has been adopted to update the weight matrix of the RBFNN model. Compared with the fixed learning intensity, the variable learning intensity has reduced initial oscillation

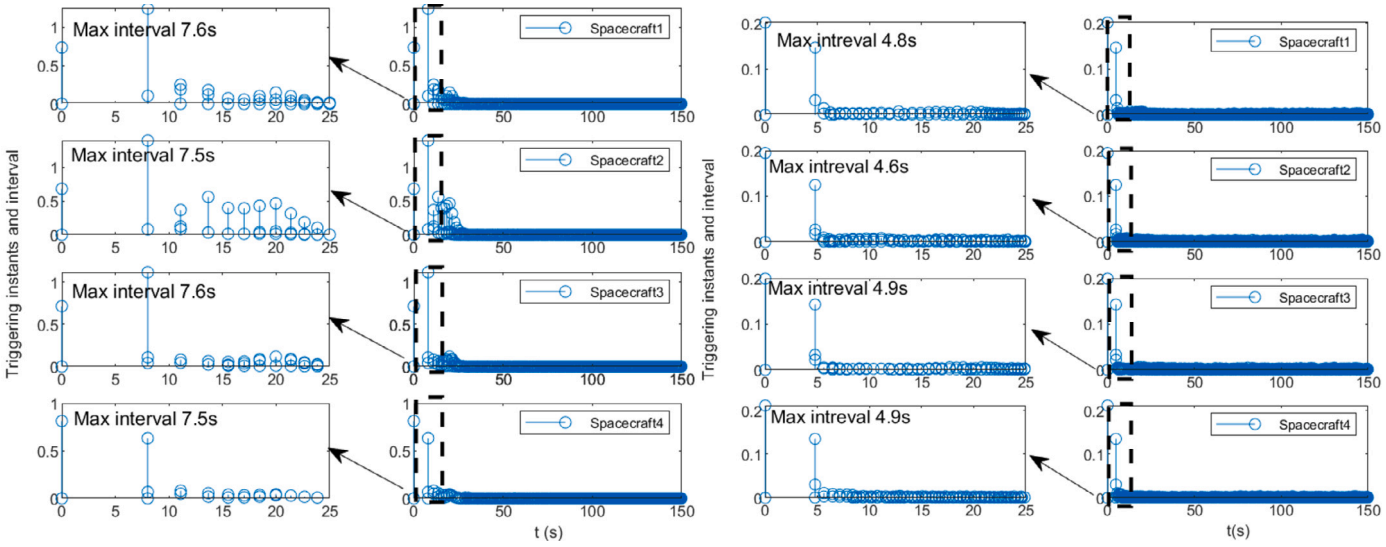

a. Example 1 a. Example 2

Fig. 13. Triggering instants and interval of four follower spacecraft in Example 1 [12] and Example 2 [14].

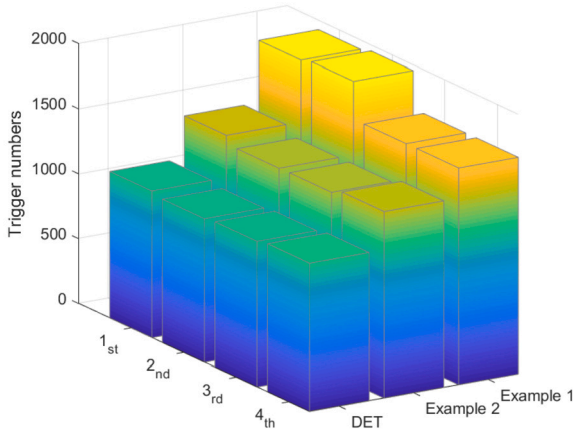

Fig. 14. Comparison of trigger numbers generated by three event-based synchronization control methods.

and weakened the saturation response by sacrificing computational resources. In addition, compared with traditional SET mechanisms, the proposed DET one has lower communication trigger numbers and more effectively avoids Zeno behavior. Finally, a series of simulation comparisons are provided to verify the effectiveness and superiority of the proposed event-based attitude synchronization control method.

Declaration of competing interest

The authors declare that they have no known competing financial interests or personal relationships that could have appeared to influence the work reported in this paper.

Data availability

Data will be made available on request.

Acknowledgements

This work is partially supported by National Natural Science Foundation of China (Grant No. 61703276, 12172168, 62003112), the Fundamental Research Funds for the Central Universities (No. JUSRP123063), 111 Project (B23008), Postgraduate Research & Practice Innovation Program of NUAA (Grant No. xcxjh20221501), and the National Research Foundation of Korea (NRF) grant funded by the Korea government (Ministry of Science and ICT) (No. NRF-2020R1A2C1005449).

References

[1] S. Mathavaraj, R. Padhi, Satellite Formation Flying, Springer, Singapore, 2021.
[2] A. Farrag, S. Othman, T. Mahmoud, A.Y. ELRaffiei, Satellite swarm survey and new conceptual design for Earth observation applications, Egypt. J. Remote Sens. Space Sci. 24 (1) (2021) 47–54.
[3] G. Di Mauro, M. Lawn, R. Bevilacqua, Survey on guidance navigation and control requirements for spacecraft formation-flying missions, J. Guid. Control Dyn. 41 (3) (2018) 581–602.
[4] G.P. Liu, S.J. Zhang, A survey on formation control of small satellites, Proc. IEEE 106 (3) (2018) 440–457.
[5] B. Cui, Y. Xia, K. Liu, Y. Wang, D.-H. Zhai, Velocity-observer-based distributed finite-time attitude tracking control for multiple uncertain rigid spacecraft, IEEE Trans. Ind. Inform. 16 (4) (2020) 2509–2519.
[6] D. Li, G. Ma, C. Li, W. He, J. Mei, S.S. Ge, Distributed attitude coordinated control of multiple spacecraft with attitude constraints, IEEE Trans. Aerosp. Electron. Syst. 54 (5) (2018) 2233–2245.
[7] B. Zhang, J. Chen, B. Hu, Distributed control of 6-DOF leader-following multi-spacecraft formation near an asteroid based on scaled twistors, IEEE Trans. Aerosp. Electron. Syst. 59 (2) (2023) 1168–1182.
[8] H. Su, X. Wang, Z. Zeng, Consensus of second-order hybrid multiagent systems by event-triggered strategy, IEEE Trans. Cybern. 50 (11) (2019) 4648–4657.
[9] X. Ge, Q.L. Han, L. Ding, Y.L. Wang, X.M. Zhang, Dynamic event-triggered distributed coordination control and its applications: a survey of trends and techniques, IEEE Trans. Syst. Man Cybern. Syst. 50 (9) (2020) 3112–3125.
[10] C. Zhang, J. Wang, R. Sun, D. Zhang, X. Shao, Multi-spacecraft attitude cooperative control using model-based event-triggered methodology, Adv. Space Res. 62 (9) (2018) 2620–2630.
[11] X. Xie, T. Sheng, L. He, Distributed event-triggered attitude consensus control for spacecraft formation flying with unknown disturbances and uncertainties, IEEE Trans. Aerosp. Electron. Syst. 58 (3) (2022) 1721–1732.
[12] F.Q. Di, A.J. Li, Y. Guo, C.Q. Xie, C.Q. Wang, Event-triggered sliding mode attitude coordinated control for spacecraft formation flying system with disturbances, Acta Astronaut. 188 (2021) 121–129.
[13] T. Wang, J. Huang, Leader-following event-triggered adaptive practical consensus of multiple rigid spacecraft systems over jointly connected networks, IEEE Trans. Neural Netw. Learn. Syst. 32 (12) (2021) 5623–5632.
[14] Y. Shi, Q. Hu, X. Shao, Y. Shi, Adaptive neural coordinated control for multiple Euler-Lagrange systems with periodic event-triggered sampling, IEEE Trans. Neural Netw. Learn. Syst. (2022), https://doi.org/10.1109/TNNLS.2022.3153077.
[15] X. Wu, S. Luo, S. Yang, C. Wei, Adaptive appointed-time formation tracking control for multiple spacecraft with collision avoidance under a dynamic event-triggered mechanism, Adv. Space Res. 70 (11) (2022) 3552–3567.

[16] G. Zhao, C. Hua, A hybrid dynamic event-triggered approach to consensus of multi-agent systems with external disturbances, IEEE Trans. Autom. Control 66 (7) (2021) 3213–3220.
[17] W. Xu, W. He, D.W. Ho, J. Kurths, Fully distributed observer-based consensus protocol: adaptive dynamic event-triggered schemes, Automatica 139 (2022) 110188.
[18] X. Tan, M. Cao, J. Cao, Distributed dynamic event-based control for nonlinear multi-agent systems, IEEE Trans. Circuits Syst. II, Express Briefs 68 (2) (2021) 687–691.
[19] B. Huang, F. Zhang, M. Song, P. Huang, Adaptive dynamic event-triggered deployment control for space triangle tethered formation system with external disturbance, Acta Astronaut. 200 (2022) 1–10.
[20] Q. Jia, J. Gao, C. Zhang, Z. Zheng, Robust relative orbit synchronization for spacecraft cluster: a distributed learning sliding mode control approach, Trans. Inst. Meas. Control (2023) 01423312231153675, https://doi.org/10.1177/01423312231153675.
[21] Q. Jia, R. Ma, C. Zhang, R. Varatharajoo, Spacecraft attitude fault-tolerant stabilization against loss of actuator effectiveness: a novel iterative learning sliding mode approach, Adv. Space Res. 72 (2) (2023) 529–540, https://doi.org/10.1016/j.asr.2023.02.041.
[22] C. Zhang, C.K. Ahn, J. Wu, W. He, Online-learning control with weakened saturation response to attitude tracking: a variable learning intensity approach, Aerosp. Sci. Technol. 117 (2021) 106981.
[23] C. Zhang, C.K. Ahn, J. Wu, W. He, Y. Jiang, M. Liu, Robustification of learning observers to uncertainty identification via time-varying learning intensity, IEEE Trans. Circuits Syst. II, Express Briefs 69 (3) (2022) 1292–1296.
[24] H. Yang, X. You, C. Hua, Attitude tracking control for spacecraft formation with time-varying delays and switching topology, Acta Astronaut. 126 (2016) 98–108.
[25] Y. Tian, Q. Hu, X. Shao, Adaptive fault-tolerant control for attitude reorientation under complex attitude constraints, Aerosp. Sci. Technol. 121 (2022) 107332.
[26] C. Zhang, M.-Z. Dai, P. Dong, H. Leung, J. Wang, Fault-tolerant attitude stabilization for spacecraft with low-frequency actuator updates: an integral-type event-triggered approach, IEEE Trans. Aerosp. Electron. Syst. 57 (1) (2020) 729–737.
[27] B. Li, Q. Hu, Y. Yang, Continuous finite-time extended state observer based fault tolerant control for attitude stabilization, Aerosp. Sci. Technol. 84 (2019) 204–213.
[28] R.Z. Chen, Y.X. Li, C.K. Ahn, Reinforcement-learning-based fixed-time attitude consensus control for multiple spacecraft systems with model uncertainties, Aerosp. Sci. Technol. 132 (2023) 108060.
[29] Q. Liu, M. Ye, J. Qin, C. Yu, Event-triggered algorithms for leader–follower consensus of networked Euler–Lagrange agents, IEEE Trans. Syst. Man Cybern. Syst. 49 (7) (2017) 1435–1447.
[30] Q. Jia, Y. Gui, Y. Wu, C. Zhang, Disturbance observer-based performance guaranteed fault-tolerant control for multi-spacecraft formation reconfiguration with collision avoidance, Aerosp. Sci. Technol. (2023) 108099.
[31] X. Wu, S. Luo, S. Yang, C. Wei, Adaptive appointed-time formation tracking control for multiple spacecraft with collision avoidance under a dynamic event-triggered mechanism, Adv. Space Res. 70 (11) (2022) 3552–3567.
[32] X. Yi, K. Liu, D.V. Dimarogonas, K.H. Johansson, Dynamic event-triggered and self-triggered control for multi-agent systems, IEEE Trans. Ind. Electron. 64 (8) (2018) 3300–3307.
[33] Q. Hu, X. Shao, Smooth finite-time fault-tolerant attitude tracking control for rigid spacecraft, Aerosp. Sci. Technol. 55 (2016) 144–157.
[34] C. Liu, G. Vukovich, K. Shi, Z. Sun, Robust fault tolerant nonfragile attitude control for spacecraft via stochastically intermediate observer, Adv. Space Res. 62 (9) (2018) 2631–2648.